Lightning Assimilation in the WRF-model (Version 4.1.1): Technique Updates and Assessment of the Applications from Regional to Hemispheric Scales

Daiwen Kang[1*], Nicholas K. Heath[2#], Robert C. Gilliam[1], Tanya L. Spero[1], and Jonathan E. Pleim[1]

[1] Center for Environmental Measurement and Modeling, Office of Research and Development, U.S. Environmental Protection Agency, Research Triangle Park, NC 27711, U.S.A.

[2] Air Quality and Atmospheric Composition, Atmospheric and Environmental Research, Lexington, MA 02421, U.S.A.

*Correspondence: kang.daiwen@epa.gov

#Currently working as an independent consultant

Abstract: The lightning assimilation (LTA) technique in the Kain-Fritsch convective

parameterization in the WRF model has been updated and applied to continental and hemispheric

simulations using lightning flash data obtained from the National Lightning Detection Network

(NLDN) and the World Wide Lightning Location Network (WWLLN), respectively. The impact

of different values for cumulus parameters associated with the Kain-Fritsch scheme on

simulations with and without LTA were evaluated for both the continental and the hemispheric

simulations. Comparisons to gauge-based rainfall products and near-surface meteorological

observations indicated that the LTA improved the model's performance for most variables. The

simulated precipitation with LTA using WWLLN lightning flashes in the hemispheric

applications was significantly improved over the simulations without LTA when compared to

precipitation from satellite observations in the Equatorial regions. The simulations without LTA

showed significant sensitivity to the cumulus parameters (i.e., user-toggled switches) for monthly

precipitation that was as large as 40% during convective seasons for monthly -mean daily

precipitations. With LTA, the differences in simulated precipitation due to the different cumulus

parameters were minimized. The horizontal grid spacing of the modeling domain strongly

influenced the LTA technique and the predicted total precipitation, especially in the coarser

scales used for the hemispheric simulation. The user-definable cumulus parameters and domain

resolution manifested the complexity of convective process modeling both with and without

LTA. These results revealed sensitivities to domain resolution, geographic heterogeneity, and the

source and quality of the lightning dataset.

1. Introduction

Thunderstorms are natural phenomena that have intrigued human imagination for

thousands of years. Although early efforts in atmospheric science and modeling were focused on

42   understanding and forecasting thunderstorms, they remain difficult to accurately simulate in

43   meteorological models. A variety of lightning parameterization schemes have developed in

44   regional and global atmospheric models (Price and Rind, 1992; Romps et al., 2014; Finney,

45   2014; Lopez, 2016) based on various physical, dynamical, and cloud properties, but these

46   schemes marginally reproduce the spatial and temporal variability of lightning flashes with

47   varying success over different regions of the globe. With the advancement of lightning detection

48   technologies both at ground level and via satellite in the past decades, observed lightning flashes

49   with coverage from regional to global scales are available and can be used for lightning

50   assimilation (LTA). A robust LTA can improve convective simulations in meteorological models

51   for retrospective atmospheric simulations (e.g., Heath et al., 2016; Marchand and Fuelberg,

52   2015) or help generate better initial fields for real-time weather forecasting (e.g., Lagouvardos et

53   al., 2013; Giannaros et al., 2016; Fierro et al., 2012, 2015) by pinpointing where deep convection

54   occurred and altering the meteorology in what is generally referred to as a hot start (Gan et al.,

55   2021). In addition, lightning also profoundly impacts the chemical composition of the

56   troposphere by generating and releasing nitrogen oxides (LNO_x) that can significantly alter

57   ground-level ozone (O_3) concentrations in some regions (Kang et al., 2020). Because

58   meteorological models drive air quality simulations, improving meteorological variables with

59   LTA will cascade to chemistry fields simulated by air quality models (Allen et al., 2012; Kang et

60   al., 2019a,b). It is especially critical when LNO_x emissions are included in air quality models,

61   since LTA is designed to align LNO_x emissions with the time and location when atmospheric

62   convection occurred in the model, so the subsequent chemistry reactions and transport will more

63   accurately reflect the emissions from lightning (Kang et al., 2019a and 2019b).

Heath et al. (2016) implemented an LTA technique in the Kain-Fritsch (KF) convective scheme (Kain, 2004) in the Weather Research and Forecasting (WRF) model, which extended the works of Rogers et al. (2000), Mansell et al. (2007), Lagouvardos et al. (2013), and Giannaros et al. (2016). In general, the lightning assimilation approach is straightforward, activating deep convection where lightning is observed and only allowing shallow convection where it is not. It was tested using WRFv3.8 simulations for several months in 2011 ~~in the Kain-Fritsch (KF) convective scheme in the Weather Research and Forecasting (WRF) model~~ using lightning observations from the National Lightning Detection Network (NLDN) over the contiguous United States (CONUS). ~~They~~ It was found that the simulation of warm-season rainfall was substantially improved, and other near-surface meteorological variables were clearly improved in retrospective WRF applications. ~~Lightning also profoundly impacts the chemical composition of the troposphere by generating and releasing nitrogen oxides (LNO$_x$) that can significantly alter ground-level ozone (O$_3$) concentrations in some regions (Kang et al., 2020). Because meteorological models drive air quality simulations, improving meteorological variables with LTA will cascade to chemistry fields simulated by air quality models. It is especially critical when LNO$_x$ emissions are included in air quality models, since LTA is designed to align LNO$_x$ emissions with the time and location when atmospheric convection occurred in the model, so the subsequent chemistry reactions and transport will more accurately reflect the emissions from lightning (Kang et al., 2019a and 2019b).~~ The LTA technique has been implemented in subsequent WRF releases (not publicly available yet) and applied in many meteorology and air quality studies over the CONUS (e.g. U.S. EPA, 2019; Appel et al, 2021). Although using LTA improved the predicted meteorological variables, some occasional unwanted departures from

86 base model predictions without LTA occurred. Most commonly, LTA resulted in a low bias in

87 summertime rainfall in some regions (U.S. EPA, 2019).

88 Heath et al. (2016) implemented the LTA technique in WRFv3.8 and tested for several

89 month simulations. The LTA technique has been implemented in subsequent WRF releases (not

90 publicly available yet) and applied in many meteorology and air quality studies over the CONUS

91 (e.g. U.S. EPA, 2019; Appel et al, 2021). Although using LTA improved the predicted

92 meteorological variables, some occasional unwanted departures from base model predictions

93 without LTA occurred. Most commonly, LTA resulted in a low bias in summertime rainfall in

94 some regions (U.S. EPA, 2019).

95 For this reason, it is of interest to investigate two parameters associated with the KF

96 convective scheme with different optional values, which are specified in the WRF runtime

97 namelist input file, are often encountered by WRF users

98 (https://www2.mmm.ucar.edu/wrf/users/docs/user_guide_v4/contents.html) . One parameter is

99 called kfeta_trigger (also referred to as trigger for simplicity in this paper) which controls the

100 conditions to determine how the KF convective scheme is triggered with three optional values: 1,

101 the default value; 2, moisture-advection based trigger (only for ARW - the advanced research

102 WRF dynamical solver); and 3, RH-dependent additional perturbation to Option 1 (not tested).

103 Another parameter is called cudt (namely **cu**mulus time interval, **d**elta **t**) and its value determines

104 the minutes between cumulus physics calls (here it is the KF scheme). The default value of 0

105 indicates that the cumulus physics is called at every model step, and any non-zero value specifies

106 the interval (minutes) that the cumulus physics is called (for example, cudt=10 means that the

107 cumulus physics is called every 10 minutes). Even though there are some discussions and

108 recommendations regarding the choice of these parameter values through online forums or WRF

109   user mailing list (e.g., https://forum.mmm.ucar.edu/; https://wrfems.info/;

110   https://www.epa.gov/sites/default/files/2017-02/documents/wrf_with_ltga_userguide.pdf), but

111   there is no literature evaluat~~inges~~ how these parameter values impact model performance when

112   LTA is used.

113   The applications and evaluations of the LTA technique were ~~Heath et al. (2016)~~

114   ~~demonstrated that the LTA techniqueconsistently improved the simulation of precipitation and~~

115   ~~other near surface variables, but the evaluation was~~ limited to the CONUS, reflecting the areal

116   coverage of NLDN (Murphy et al., 2021). As the spatial applications of atmospheric composition

117   modeling are expanded from regional to hemispheric and global scales and new lightning

118   datasets are available, there is a strong need to examine how this LTA technique performs at

119   these larger scales when lightning flash data from a less accurate detection network are used.

120   Thus, lightning flashes from the World Wide Lightning Location Network (WWLLN, operated

121   by the University of Washington: http://www.wwlln.com) is a suitable candidate because it has

122   the global coverage ~~with affordable cost~~, albeit its detection efficiency is lower than the >95% of

123   NLDN for cloud-to-ground (CG) flashes (Abarca et al., 2010).

124   Our research has multiple objectives based on the aforementioned open research needs:

125   1) assess the impact of the parameter values associated with the KF convective scheme on WRF

126   performance over the CONUS domain without LTA (BASE case) and with LTA using lightning

127   flashes from NLDN; 2) examine the LTA in WRF using lightning flashes from WWLLN and

128   compare to the simulations with NLDN lightning flashes; and 3) apply LTA to WRF simulations

129   over the Northern Hemisphere and evaluate the performance in terms of precipitation and near-

130   surface meteorological variables. In section 2, we describe the updates made to the initial LTA

131   technique (Heath et al., 2016). Section 3 provides the detailed data and methodologies of the

132 model simulations and their evaluation. Section 4 presents our analysis on the impact of

133 parameters with KF convective schemes with and without lightning assimilation over CONUS

134 using lightning flashes from NLDN and WWLLN. In section 5, we analyze the use of lightning

135 flashes from WWLLN for LTA and evaluate WRF simulations with and without LTA over the

136 Northern Hemisphere. And we conclude with key findings and recommendations in section 6.

2. Updates on the LTA technique

138 The lightning assimilation used here is based on Heath et al. (2016), and ~~which extended~~

139 ~~the works of Rogers et al. (2000), Mansell et al. (2007), Lagouvardos et al. (2013), and~~

140 ~~Giannaros et al. (2016). In general, the lightning assimilation approach used here is~~

141 ~~straightforward, activating deep convection where lightning is observed and only allowing~~

142 ~~shallow convection where it is not. This method is applied in the Kain-Fritsch scheme in WRF~~

143 ~~(Kain, 2004). A~~a full description of the method can be found in Heath et al.~~ (2016)~~. Here, we

144 provide only the essential details, along with recent modifications to the scheme.

145 First, the lightning data (WWLLN or NLDN) is binned to the WRF domain in both time

146 and space. The temporal binning is done every 30 min and includes lightning data from -10 min

147 to +20 min of the current time. The spatial regridding searches for a lightning strike within each

148 grid box (using the staggered grid edge coordinates) within each time bin. This process creates a

149 new lightning file with the same horizontal dimensions as the WRF domain filled with zeros (no

150 lightning) or ones (lightning) at each 30-minute time step. ~~–~~During the WRF simulation, if

151 lightning is present, the scheme first goes through its standard updraft calculations, except that it

152 uses the layer with the greatest moist static energy as its updraft source layer (USL). If the

153 resulting cloud does not meet the criteria for deep convection, 0.1 g kg^{-1} of water vapor and 0.1

154 K are incrementally added to the USL until deep convection is forced. In the original Heath et

155 al. scheme, only moisture was added to the USL. We have included temperature perturbations to

156 further promote activating deep convection in these grid points with lightning.

157   In the unmodified KF scheme, a cloud must exceed a minimum depth (as a function of

158 cloud base temperature) to satisfy the deep convection criteria. Specifically, a cloud base

159 temperature greater than 20-°C must have a cloud greater than 4 km deep. For a cloud base

160 temperature less than 0-°C, the cloud depth only needs to be 2 km. For cloud bases between 0 –

161 20-°C, the minimum cloud depth is defined as $2000 + 100T_{LCL}$, where T_{LCL} is the temperature at

162 the lifted condensation level (LCL) (Kain 2004). Heath et al. (2016) modified this depth for

163 lightning assimilation to be more consistent with lightning-producing storms. Specifically,

164 within WRF, storms with a base temperature greater than or equal to 20°C must have a cloud

165 depth of at least 6 km with a cloud top temperature less than -20°C. Similarly, in the original

166 model in Heath et al., storms with a cloud base temperature less than 20°C must have a cloud

167 depth of at least 4 km and a cloud top temperature less than -20°C. These criteria were set to

168 ensure that sub-grid deep convective clouds were deep enough to have a mixed-phase layer to

169 support lightning (e.g., Mansell et al., 2007; Bruning et al., 2014; Preston and Fuelberg, 2015).

170 In this study, we slightly modified the scheme to require that the cloud top is at least one model

171 level above the -20°C level, ensuring cloud-top temperatures are less than -20°C (e.g.,

172 Stolzenburg and Marshall, 2009). The prior limit at -20°C could inadvertently weaken simulated

173 deep convective clouds, which may contribute to the dry bias in earlier applications of lightning

174 assimilation approaches (U.S. EPA, 2019).

175   In Heath et al. (2016), if deep convection could not be achieved after incrementally

176 adding up to 1 g kg^{-1} to the USL (which is now 1 g kg^{-1} and 1 K in our update), then no further

177 action was taken, and deep convection was not activated by KF. However, to increase the

178   realism of the scheme and increase the odds of deep convection the next time the scheme is

179   called, we have updated the approach as follows. If a deep convective cloud cannot be activated,

180   the tallest cloud created is passed into the KF shallow convection scheme. In the KF scheme,

181   shallow clouds are re-diagnosed each time the scheme is called. For example, suppose a shallow

182   cloud is generated at t=0 and KF is called at 5 min intervals. In that case, at the t=5 min call, KF

183   would determine if a shallow cloud is still present. Thus, the cloud can evolve so that at t=5 min

184   it could have slightly different characteristics than the one diagnosed at t=0. This allows shallow

185   clouds to grow, decay, or persist at short timescales.

186   Therefore, if the LTA method cannot trigger deep convection, the shallow cloud that is

187   generated within WRF can precondition the atmosphere, thus increasing the likelihood of deep

188   convection the next time the KF scheme with LTA is called. Therefore, these refinements to the

189   LTA scheme in KF more closely replicate how convective initiation is observed in nature, where

190   shallow cumulus and congestus clouds precondition the environment prior to deep convection

191   initiation.

192   Lastly, at grid points without observed lightning, deep convection is suppressed in WRF,

193   and only the shallow portion of KF is allowed to run (this is referred to as the "ShallowOnly"

194   method). Because convective clouds in nature can form and precipitate without generating

195   lightning, this suppression technique serves as a realistic approach to reproduce nature given the

196   constraints of the KF parameterization.

197

198   **3. Data and Methodology**

199   3.1. Lightning flash data

200   Lightning flash data from two ground-based lightning detection networks were used for the

201   assimilation using the LTA technique in this study. The NLDN provides cloud-to-ground

202   lightning observations with a detection efficiency of >95% and a location accuracy of about 150

203   m (Murphy et al., 2021) over the contiguous U.S. (CONUS). The WWLLN provides global

204   lightning data with lower detection efficiency and location accuracy (Abarca et al., 2010;

205   Rudlosky and Shea, 2013; Burgesser, 2017) compared to NLDN and the Lightning Imaging

206   Sensor (LIS) observations (Mach et al., 2007). Since WWLLN has global coverage, even with its

207   relatively lower detection efficiency and location accuracy compared to NLDN, it could be a

208   good option for applications beyond CONUS. Figure 1 shows how the average lightning flash

209   rate (flashes $km^{-2}hr^{-1}$) from WWLLN compares to NLDN during July and September 2016 when

210   hourly lightning flash counts are gridded into the CONUS 12-km grid cells.

211   As shown in Figure 1, the lightning flash rates in NLDN are much higher than those in

212   WWLLN, especially during July and over the land, and this is generally true (not shown) that

213   NLDN reported more lightning flashes than WWLLN during warm months over land. The

214   differences are much smaller during cool months and over the coastal regions where NLDN has

215   coverage. Note that the absolute difference in flash count may not necessarily translate

216   proportionally into convective activities in terms of LTA because the LTA technique as

217   described in Heath et al. (2016) depends on the detection of lightning occurrence (binary "yes"

218   or "no" situation), not the actual flash count, in a specific time interval at a grid cell.

219   3.2. Precipitation Data

220   The daily precipitation from the Parameter-elevation Regressions on Independent Slopes

221   Model (PRISM)'s high-resolution spatial climate data for the United States

222   (https://climatedataguide.ucar.edu/climate-data/prism-high-resolution-spatial-climate-data-

223 united-states-maxmin-temp-dewpoint) is used to evaluate WRF-simulated precipitation over the

224 CONUS, and the NOAA Climate Prediction Center (CPC)'s global unified gauge-based analysis

225 of daily precipitation (https://psl.noaa.gov/data/gridded/data.cpc.globalprecip.html) product is

226 employed to assess WRF's hemispheric precipitation predictions. The daily total PRISM

227 precipitation data are available at 4-km horizontal grid spacing over the CONUS, and the annual

228 CPC precipitation (partitioned into daily totals) is available globally at $0.5°$ latitude $× 0.5°$

229 longitude grid $(720 × 360)$ resolution. These datasets were regridded to the WRF modeling

230 domains for the 12-km CONUS and the 108-km Northern Hemisphere to pair with model

231 simulations in time and space. To assess the simulated precipitation over the oceans, especially

232 in the tropical regions where no gauge-based measurement is available, products from the Global

233 Precipitation Measurement (GPM) (Huffman et al., 2015; Asong et al., 2017), a joint mission co-

234 led by NASA and the Japan Aerospace Exploration Agency (JAXA) and comprised of an

235 international network of satellites that provide the next-generation global observations of rain

236 and snow, are employed. The Integrated Multi-satellitE Retrievals for GPM (IMERG) Long-term

237 Precipitation Data Products

238 (https://arthurhouhttps.pps.eosdis.nasa.gov/gpmdata/YYYY/MM/DD/imerg/; registration is

239 required for access) cover the entire globe with $0.1°$ latitude $× 0.1°$ longitude grid resolution. To

240 compare with WRF simulated hemispheric precipitation, the daily mean precipitation data from

241 the IMERG V06 dataset (https://gpm.nasa.gov/data/directory) from 2016 is regridded onto the

242 hemispheric WRF domain (https://gpm.nasa.gov/data/directory). The research-quality gridded

243 IMERG V06 dataset Final Run product estimates precipitation using quasi-Lagrangian time

244 interpolation, gauge data, and climatological adjustment.

245 3.3. Ground-Based Meteorological Data

246   The impacts of user-definable parameter values associated with KF and datasets for LTA

247   were quantified for simulated near-surface meteorological variables such as precipitation, 2-m

248   temperature (T2), water vapor mixing ratio, wind speed and wind direction. The simulated

249   meteorological fields from WRF are compared against observations from NOAA National

250   Centers for Environmental Information (NCEI) land-based stations, which are archived from

251   data collected globally (https://www.ncei.noaa.gov/products/land-based-station). The

252   Atmospheric Model Evaluation Tool (AMET) (Appel et al., 2011) is used to pair surface

253   observations with model predicted values in both space (bilinear interpolation) and time (hourly).

254   3.4. Model Configurations and Simulation Details

255   The WRF model (Skamarock and Klemp, 2008) version 4.1.1 (WRFv411,

256   https://github.com/wrf-model/WRF/releases/tag/v4.1) with LTA updates to Heath et al. (2016)

257   (as described in Section 2) is used to perform simulations over the CONUS and the hemispheric

258   domains. The CONUS domain is configured with 36 vertical levels and 12-km horizontal grid

259   spacing with 472×312 grid points. The hemispheric domain is configured with 45 vertical

260   levels and 108-km horizontal grid spacing with 200×200 grid points that covers the entire

261   Northern Hemisphere and the northern border of the Southern Hemisphere along the Equator.

262   The simulation period for CONUS simulations is from April–July in 2016 with 10-day spin-up

263   period from March 22; for the hemispheric domain, annual simulations for 2016 are performed.

264   Our analysis focuses on July when convective activities are often the most prevalent over the

265   CONUS; other months are examined in the hemispheric simulations which simulate the year-

266   round convective activities in the tropics. The detailed configurations of cloud microphysics,

267   land surface parameters, radiation schemes, and four-dimensional data assimilation (FDDA) are

268   the same as described in Heath et al. (2016) and sample WRF namelist input files for both the

269 CONUS and hemispheric simulations are included in the supplementary information (Table S1

270 and Table S2). Data assimilation in the form of FDDA more specifically follows Heath et al.

271 (2016) with updates noted in Gilliam et al. (2021) for the hemispheric domain where ~28 km

272 NCEP Global Forecast System (GFS) analyses were used to nudge tropospheric temperature,

273 moisture, and wind above the planetary boundary layer. For the CONUS domain the same

274 nudging was applied, but 12 km North American Mesoscale (NAM) model analyses were

275 leveraged. These two analysis datasets are a blend of short-term forecast with a comprehensive

276 set of surface, upper-air, radar, aircraft, satellite, and other observations like sea-surface

277 temperature that represent the best guess of the state of the atmosphere at any given time.

278   The KF scheme includes two options to trigger convective activity. Trigger 1 is based on

279 a mass-conservative cloud model, which includes parameterized moist downdrafts, entrainment,

280 and detrainment at the cloud edge (Kain and Fritsch, 1990, 1993) and allows interaction between

281 cloud and environment, and it is the default option for most applications. Trigger 2 is an alternate

282 option based on Ma and Tan (2009), and that is a moisture-advection modulated trigger function

283 to improve results in subtropical regions when large-scale forcing is weak. In addition, the KF

284 scheme is called by default at every time step, but it can be configured to only update convective

285 parameters on a user-definable time increment. In this study, sensitivities are conducted to the

286 version of the KF trigger (i.e., Trig1 and Trig2, abbreviated as K1 and K2 in Table 1,

287 respectively), as well as to frequency at which KF is called (i.e., "cudt"). Two sensitivities on

288 cudt were performed: one where KF is called at each model integration time step (i.e., "Cudt0",

289 abbreviated as C0 in Table 1), and the other where KF is updated every 10 minutes of integration

290 time (i.e., "Cudt10", abbreviated as C10 in Table 1). The time step is 1 minute (Table S1) and 3

291 minutes (Table S2) for the CONUS and hemispheric WRF simulations, respectively. The

292   sensitivities to KF trigger and update frequency are combined in a matrix of simulations that also

293   are conducted with/without LTA, and they are listed in Table 1. All eight simulations are

294   performed for both the CONUS and the hemispheric domains. For LTA cases, lightning flashes

295   from both NLDN and WWLLN are used over the CONUS domain and lightning flashes from

296   WWLLN are used for the hemispheric domain. For convenience of description, the cases without

297   LTA are collectively referred to as BASE cases, and the cases with LTA are referred to as LTA

298   cases. To further distinguish the lightning networks, the LTA cases are also referred to as LTA

299   NLDN (or simply NLDN) and LTA WWLLN (or simply WWLLN) cases, respectively.

300   3.5. Evaluation Methodologies

301   The assessment of the impact of LTA on model performance is focused on precipitation

302   since that is the most affected variable, though other near-surface variables are also evaluated.

303   Due to the highly heterogeneous nature of thunderstorms and lightning over space, in addition to

304   examining the overall statistics across the modeling domain, statistics are analyzed to assess the

305   impact of LTA over U.S. climate regions (https://www.ncei.noaa.gov/monitoring-

306   references/maps/us-climate-regions) in both domains and some of the larger countries in the

307   hemispheric simulations. Figure 2 shows these climate regions over the CONUS modeling

308   domain and the selected countries (also referred to as regions) in the hemispheric modeling

309   domain.

310   The statistical metrics in this analysis include the widely used correlation coefficient (r)

311   to measure the linear association of measured and simulated variables, mean bias (MB) and

312   normalized mean bias (NMB) to quantify the departure of simulated values from measured

313   values, and root mean square error (RMSE) and normalized mean error (NME) to elucidate the

314   errors associated with model simulations. More emphasis is placed on certain metrics than others

315 depending on the nature of the simulated quantity. For instance, with precipitation, correlation

316 coefficient (if the model can simulate rainfall at the right time and location) and MB and NMB

317 (if the model over- or under-estimate rainfall amount) are more straightforward than the error

318 metrics (though they are still relevant), but MB and NMB are inappropriate to evaluate wind

319 directions.

320

321 **4. CONUS WRF Simulations**

322   As shown in Table 1, four BASE (without LTA) cases, four LTA cases using lightning flash

323 data from NLDN, and four LTA cases using lightning flash data from WWLLN over the

324 CONUS domain were performed using the combinations of two trigger options and two

325 convective update (cudt) intervals, respectively. For the LTA cases, when lightning flashes were

326 not present, the ShallowOnly option (Heath et al., 2016) was used (Table S1).

327 4.1. Precipitation

328   Figure 3 displays the July 2016 mean statistics generated by pairing the gridded WRF

329 precipitation with the values from PRISM in time and space for each of the U.S. climatological

330 regions. As shown in Figure 3, the BASE simulations present the more most dramatic

331 fluctuations among cumulus parameter sensitivities than the LTA cases. With Trig1, when the

332 cudt is changed from 0 to 10, the correlation coefficient is substantially reduced across all the

333 regions (Figure 3a), and increases in biases (overestimate of precipitation, Figures 3b&c) and

334 errors (Figures 3d&e) are also worsened by less frequent cumulus updates. With trigger 2, the

335 biases (MB and NMB) changed from overestimation to underestimation, and the errors (RMSE

336 and NME) were smaller compared to Trig1. Though the setting for cudt altered simulations with

337 Trig2, the difference was smaller than the cases with Trig1. In general, the Trig1 cases tended to

338   produce more precipitation (overestimate compared to PRISM precipitation) than the Trig2 cases

339   (underestimate compared to PRISM precipitation), and the Cudt10 cases generated more

340   precipitation than the Cudt0 cases. Among the four cases in the BASE model simulations, the

341   K1C0 case (Trig1, Cudt0) is the most favorable in terms of the correlation coefficients and

342   precipitation biases, but the error statistics, especially NME, may not be the most desirable.

343   Using LTA (Figure 3), the correlation coefficients significantly increased over the

344   domain and across the regions (from the range of ~0.25 to ~0.40 to the range of ~0.30 to ~0.48)

345   relative to the BASE cases. Though the LTA WWLLN cases had lower correlation compared to

346   the LTA NLDN cases due to the lower detection efficiency of lightning flashes in WWLLN, the

347   improvement was still rather considerable compared to the BASE cases. The biases in the LTA

348   NLDN cases are most favorable with values negative but closest to zero (small underestimate).

349   The LTA WWLLN cases produced larger negative biases than the BASE cases and LTA NLDN

350   cases, again, related to detection efficiency of the networks. All the LTA cases (both NLDN and

351   WWLLN) produced smaller errors than the BASE cases, and the differences between the NLDN

352   cases and WWLLN cases were minimal. Comparing the LTA cases with the BASE cases, one

353   noticeable feature is that with the different trigger and cudt values, all the statistics fluctuated

354   dramatically from one case to another in the BASE cases, but fluctuation among the LTA cases

355   was minimized and negligible. This is expected, as the moisture and temperature perturbations

356   used to trigger convection with LTA (Section 2) will take precedence over the trigger options

357   and grouping the lightning data into 30-minute bins should mitigate the influence of the cudt

358   option. These features were deliberately incorporated into the LTA technique for precisely these

359   reasons, but this paper documents their systematic testing.

360 Examination of the statistics across the climatological regions over the CONUS domain

361 indicates that the Ohio Valley (OVC) stands out among all the regions with the lowest

362 correlation coefficients and largest RMSE values in all the BASE cases. However, with LTA, the

363 correlation coefficients in OVC were brought to the median range among other regions, though

364 the RMSE values were still the largest in that region; these features in OVC are more

365 understandable as manifested in Figure 12, examined in detail in Section 5. Other statistics in

366 OVC with LTA were comparable with other regions except for relatively larger negative MB

367 values associated with the LTA WWLLN cases. Another obvious characteristic with regards to

368 correlation coefficients and errors (RMSE and NME) was that there was more spread among the

369 regions in the LTA cases than in the BASE cases (except in OVC), which resulted from the

370 geographically heterogeneous nature of convective precipitation and the associated observed

371 lightning intensity across the regions.

372 To alleviate the underestimation of precipitation in the LTA WWLLN cases, additional

373 simulations (K1C10Ws0 and K2C10Ws0; where K1C10W and K2C10W are the same as in

374 Table 1, while s0 means zero suppress when lightning flash is not present) were performed by

375 switching the suppression option as described in Heath et al. (2016) from "ShallowOnly" to

376 "NoSuppress." This modification still triggers deep convection where lightning is observed;

377 however, at grid points without lightning, the KF scheme is configured to run normally (i.e., the

378 same as in the BASE cases). As shown in Figure S1, the correlation coefficients in the

379 WWLLN+s0 cases were comparable with other LTA cases, and the values in the K2C10Ws0

380 case were similar to the NLDN cases and improved upon the K1C10W case. The MB in the

381 WWLLN+s0 cases were mostly positive (overestimate), which is expected because the KF

382 scheme has more freedom to activate deep convection. The K2C10Ws0 case produced the most

383   desirable results (domain mean MB is nearly zero) among all the cases. However, the biases

384   associated with LTA simulations using the "NoSuppress" option are affected by both the

385   lightning detection efficiency and the domain resolutions, which is more evident in the LTA

386   simulations over the hemispheric domain in Section 5.

387   4.2. Other Near-Surface Meteorological Variables

388   Besides precipitation, T2, water vapor mixing ratio, wind speed, and wind direction are

389   also analyzed. As shown in Figure 4, T2 in the BASE cases has correlation coefficients over the

390   CONUS domain and all the regions ranging from ~0.95–0.98. With LTA, the correlations for T2

391   were further improved for all the regions, with WWLLN cases performing slightly worse than

392   the NLDN cases. The impact of cumulus parameters on correlations was minimal for the BASE

393   and LTA cases. However, the cumulus parameters seem to impact the biases (MB and NMB,

394   Figures 4b,c) and errors (RMSE and NME, Figure 4d,e) in the BASE cases across all the regions,

395   and like precipitation, all the LTA cases minimized the impact of different cumulus parameter

396   values. All the LTA cases reduced the errors (RMSE and NME) associated with T2 across all the

397   regions, with NLDN slightly better than WWLLN. In summary, the T2 statistics were improved

398   by using LTA, and the WWLLN cases were comparable to the NLDN cases with a slight

399   degradation for all the regions.

400   The 2-m water vapor mixing ratios metrics (Figure 5) of the cases, in general, resemble

401   those of T2, in that the LTA cases have slightly increased the correlation coefficients from the

402   already well-simulated BASE cases. More spread occurs for biases (MB and NMB, Figures 5b,c)

403   and within the BASE cases for errors (RMSE and NME, Figures 5d,e). Regional spread in these

404   statistics is attributed to the diverse air mass types that drive large differences in the moisture

405   content and convective activity. Even though the values were low for both errors and biases (<

406   0.5%), using either LTA technique is an improvement over the BASE cases.

407   The cumulus parameters and LTA showed less impact on the correlations for 10-m wind

408   speed, but the impacts on biases and errors were noticeable (Figure 6). All the model cases

409   underestimate wind speed (~5–12%, depending on regions and model cases), and the cumulus

410   parameters caused relatively large differences in the metrics of the BASE cases with both trigger

411   and cudt options contributing most. Overall, using Trig2 with Cudt10 is most favorable in terms

412   of biases (less underestimate) and errors (smaller errors) among the BASE cases. In all the LTA

413   cases, the underestimation was reduced when compared to the BASE cases, and errors were

414   reduced with negligible differences among the cases with different cumulus parameters and

415   assimilating lightning data from the different networks. Similar behavior was observed for wind

416   direction where only correlation coefficient, MB, and RMSE are displayed in Figure S2 because

417   normalized metrics do not apply.

418

419   **5. Northern Hemispheric WRF Simulations**

420   As shown in Table 1, the model cases performed over the Northern Hemisphere are

421   similar to those performed over the CONUS, but with LTA cases using lightning data from

422   WWLLN that was gridded on the domain with 108-km horizontal grid spacing.

423   5.1. Precipitation

424   Before comparing the simulated precipitation with available observations, the examination

425   begins with how the WRF-simulated precipitation with and without LTA compares spatially over

426   the Northern Hemisphere. Figure 7 displays the mean daily precipitation during July 2016 from

427   two LTA cases and two BASE cases (Trig1 and Trig2) and the corresponding differences between

428   LTA and BASE (LTA – BASE) cases with the same trigger values, and Figure S3 presents the

429   mean daily precipitation differences between HK1C0W and HK1C0B cases throughout 2016.

430   Compared to the BASE cases, the LTA cases produced significantly less rainfall along the

431   Equatorial regions but generally more rainfall away from the Equator, especially over the

432   midlatitude land regions. Because no gauge-based observational data are available over the ocean,

433   the IMERG precipitation for July 2016 is presented in Figure 7g with the difference plots from the

434   base case (HK1C0B) and the LTA case (HK1C0W) being displayed in Figures 7h and 7i,

435   respectively. Over the Equatorial regions, the precipitation simulated by the LTA cases (Figures

436   7b and 7e) more closely resembled the IMERG precipitation than the BASE cases. The difference

437   plots clearly indicate that the base cases significantly overestimated, and the LTA cases slightly

438   underestimated the precipitation over large areas in the Equatorial regions. Similar results persisted

439   throughout the year as shown in Figure S4 (the difference of mean daily precipitation by month

440   between the base case, HK1C0B, and the IMERG product) and Figure S5 (the difference of mean

441   daily precipitation by month between the LTA case, HK1COW, and the IMERG product). Next,

442   the WRF simulated precipitation is compared with the CPC gauge-based analysis values over land.

443   Figure 8 displays the CPC rainfall and simulated mean daily precipitation during July 2016 along

444   with the estimates from the LTA and BASE cases with different cumulus parameters. Since the

445   gauge-based observational values are only available over land, the simulated values in Figure 8

446   are only displayed over land. As shown in Figure 8, all the model cases simulated the overall

447   spatial pattern of higher values in the tropical regions and lower values in high latitude regions.

448   However, subtle differences existed from case to case in different regions. For example, the

449   HK1C10B case (Figure 8d) and the HK2C10B case (Figure 8f) produced the highest and the lowest

450   precipitation over Africa and South America (along the Mexico coast to the South American

451   continent) within the modeling domain.

452   All the LTA cases uniformly produced larger correlation coefficients than the BASE

453   cases (Figure 9) when and where convective activities were prevalent. In the U.S., convective

454   activities occur during warm months (from May to September), while in Mexico and India,

455   convection is active throughout the year. In Canada, convective activities are less frequent

456   because of the cooler temperatures and low moisture at the high latitude. When and where

457   convection was active, the cumulus parameters produced significant differences in modeled

458   convective activity, as correlation coefficients are higher in the BASE cases with Trig1. Same as

459   the simulations over the CONUS domain, the cumulus parameters had a minor impact on the

460   correlation coefficients for the LTA cases regardless the regions. This indicates that, even with

461   the less dense WWLLN lightning observations, using LTA improves the timing and location of

462   deep convection.

463   RMSE were comparable for all the model cases across the selected regions (Figure 10),

464   with the LTA cases pointing to lower values than the BASE cases at all the regions except for the

465   U.S. where the LTA and BASE cases alternated to have slightly lower RMSE values over each

466   other during the year. Alternatively, the MB values varied significantly among the model cases

467   and across the regions as shown in Figure 11. One common feature is that the differences among

468   the LTA cases were small, but two distinctly separate groups among the BASE cases were noted

469   in all the regions; the cases with Trig1 had always significantly greater precipitation values than

470   the cases with Trig2. In China and Mexico, all the simulations overestimated the precipitation

471   through the year except for small underestimate during the cool months (October–December). In

472   India, the overestimate and underestimate were equally split among the model cases, with

473 dramatic changes from month to month in the same model case. The behavior of MB values

474 among the model cases and through the year was more stable for the U.S. (to a lesser extent in

475 Canada) than in other regions, in which the BASE cases with Trig1 have the best performance

476 (MB values near zero), the BASE cases with Trig2 significantly underestimated precipitation

477 over land during convective season, and all the LTA cases overestimated precipitation over land

478 during the warm months. Here we offer two plausible explanations for the drastically different

479 behaviors of the MB values associated with precipitation in different regions.

480 First, from the modeling point of view, the WRF model is widely studied and applied in

481 North America, especially in the U.S. As a result, more accurate observation-based datasets are

482 available to nudge WRF through FDDA (Liu et al., 2008), and all the work has led to the best

483 performance over the U.S. for the recommended default set of convective trigger and update

484 frequency for the cumulus scheme. Second, from the observational point of view, the CPC

485 rainfall dataset is built upon field gauge measurements that may vary in accuracy and

486 consistency from county to county. As shown in Figure S6, the NMB values were generally in

487 the range of -50% to 50% in the U.S. and Canada (comparable to the NMB values for the 12-km

488 CONUS simulations against PRISM precipitation as shown in Figure 3c), but in other countries,

489 especially during cool months, the values were up to hundreds or even thousands of percent that

490 suggests possible few observations available in the denominator in NMB calculations. For

491 instance, the highest NMB value in China coincided with the Spring Festival that is often a long

492 holiday for China suggesting possible gaps for data collection.

493 We next focus on the high MB values associated with the LTA cases in the U.S.

494 Consistent with in the analysis in Figure 3b, the LTA WWLLN cases over the 12-km CONUS

495 domain always had larger negative MB (underestimates) than the LTA NLDN cases due to the

496 lower detection efficiency of lightning flashes in WWLLN than in NLDN. However, in the 108-

497 km hemispheric simulations, the same WWLLN datasets produced large positive MB

498 (overestimates) for precipitation. To understand this phenomenon, we need to first examine how

499 the LTA method works. Because it uses a yes/no lightning indicator to trigger convection, 108-

500 km grid spacing might be too coarse for such a simplistic approach to work. For example, one

501 lightning strike within a 108-km grid cell will trigger deep convection, which, because of the

502 large spatial coverage of the grid cell, can contribute to the high bias in precipitation because

503 convective rainfall is realistically more localized. Although the KF scheme sets a fixed radius

504 for thunderstorms (e.g., Equation 6 in Kain 2004), applying the resulting rain over the entire 108-

505 km $\times$ 108-km grid box could partially explain the excess rainfall. This may also be explained by

506 the fact that the convective time-scale formulation in KF scheme was originally developed at

507 grid lengths of 20–25 km (Sims et al., 2017). A potential developmental pathway for the LTA

508 method at these scales is to test different thresholds of the 30-min flash density to ensure

509 sufficient lightning is present to trigger deep convection. Overall, compared to the CPC rainfall,

510 the LTA technique significantly improved the temporal and spatial correlation of convective

511 precipitation, but the precipitation amount was overestimated over the U.S. and other regions for

512 the 108-km modeling domain.

513   To further examine the impact of modeling domain resolutions on convective

514 precipitation, Figure 12 displays the spatial precipitation from PRISM, CPC (regridded onto the

515 12-km CONUS domain), and simulated precipitation from one BASE case and two LTA cases

516 with NLDN and WWLLN data, respectively, over the 12-km CONUS domain and one LTA case

517 over the 108-km hemispheric domain that has been regridded to the 12-km CONUS domain. As

518 shown in Figures 12a,b, the two observation-based precipitation products, PRISM and CPC,

519   compared well to each other, noting that the PRISM product displays more subtle granularity

520   than the CPC product due to the large difference in spatial resolutions (4-km for PRISM versus

521   0.5° for CPC). The overall spatial pattern of mean daily precipitation was captured by both the

522   12-km LTA simulations (Figures 12d,e), and the 108-km LTA simulation (Figure 12f). The

523   heaviest rainfall was centered in the OVC area in the observation-based and the simulated

524   precipitation maps, but the shape and spread of the rain band were different. The rain band in the

525   12-km BASE case (Figure 12c) was more spread and scattered with southwest-to-northeast

526   orientation, while the observation-based products and the LTA cases indicated a relatively

527   smaller area with west-east direction. Thus, the LTA cases (12-km CONUS simulations)

528   compared better to the observation-based products spatially than the BASE case. The K2C10W

529   case (with WWLLN) tended to produce less precipitation than the K2C10N case (with NLDN)

530   and both observation-based products. These spatial discrepancies for precipitation in OVC

531   between PRISM and the model cases were reflected by the unique statistical behavior as

532   displayed in Figure 3 and discussed in Section 4.1. As a likely artifact of excessively activated

533   convection within the 108-km grid cells with a spatial scale much larger than most thunderstorm

534   scales, the HK2C10W case indicated areas of heavy precipitation that were also shown in the

535   observation-based products and the 12-km LTA cases (both K2C10W and K2C10N) at

536   approximately same locations but with much less spatial extent. To resonate with the large

537   discrepancies in the MB values shown in Figure 11a among the BASE cases, the precipitation

538   from HK2C10B and HK2C10B cases is similarly displayed in Figures 12g,h. The case with

539   Trig1 was clearly more comparable to the CONUS cases than the Trig2 case in that the

540   precipitation from Trig2 was severely underestimated across the entire U.S. These hemispheric

541   simulations amplified the impact of the trigger options on precipitation during warm months

542   among the BASE cases, resulting in differences in daily total precipitation of up to 40% in the

543   U.S. (Figure S6a). These results underscore the need to carefully set cumulus parameters for the

544   KF scheme in WRF simulations.

545   The mismatch of the spatial scales between domain resolution and thunderstorms in the

546   108-km simulations is a limitation of current LTA scheme that could be improved in future

547   development. In addition to using lightning density to trigger convection, another option is to

548   implement the LTA scheme in the MultiScale Kain-Fritsch (MSKF) scheme (Glotfelty et al.,

549   2019; Zheng et al., 2016), a "scale-aware" variant of KF that refines the convective tendencies

550   based on the grid spacing used in the simulation.

551   5.2. Impact on Other Meteorological Variables

552   The impact of the cumulus parameters and LTA scheme on near-surface meteorological

553   variables of the 108-km hemispheric simulations are evaluated like the 12-km CONUS

554   simulations. However, due to the lack of observation data beyond North America, the analysis is

555   mainly focused on the U.S. regions, but all the available data within the hemispheric domain is

556   collectively referred to as "ALL" regardless of where the data originated. Affected by the coarser

557   domain resolution, all the statistical measures for T2 (Figure 13) from the hemispheric

558   simulations indicated degradations in model performance relative to the 12-km CONUS domain

559   (Figure 4). As in the CONUS simulations, the LTA cases increased correlation coefficients and

560   decreased errors (RMSE and NME) compared to the BASE cases. Like the CONUS simulations,

561   the cumulus parameters minimally affected the LTA cases, while significant deviations were

562   produced among the BASE cases. Unlike the CONUS simulations where both trigger and cudt

563   contributed to T2 differences, the large differences among the BASE cases for the hemispheric

564   simulations were attributed to the trigger options. Though all the cases tended to underestimate

565   T2 (contrary to the CONUS simulations where T2 was generally overestimated), among the

566   BASE cases, greater underestimates were associated with Trig1 than Trig2. The LTA cases

567   uniformly underestimated T2 consistent with the Trig1 BASE cases. The performance of

568   hemispheric simulations for 2-m water vapor mixing ratio (Figure 14) resembles T2 in the

569   comparison to the CONUS simulations (Figure 5), which produced smaller correlation

570   coefficients and larger errors and biases (mainly overestimates for both CONUS and hemispheric

571   simulations). Without exception, the LTA cases consistently performed better in terms of

572   correlation coefficients and errors than the BASE cases. However, different from other

573   meteorological variables, the MB and NMB associated with water vapor mixing ratio are

574   affected by both cumulus parameters (trigger and cudt) for all the model cases (both BASE cases

575   and LTA cases). The LTA cases with Trig1 performed better than the cases with Trig2, and with

576   the same trigger value, cudt=0 is preferable to cudt=10; however, for the BASE cases, it was the

577   opposite, though with smaller differences. At the 108-km grid spacing, the 10-m wind speed

578   (Figure S7) and wind direction (not shown) statistics were comparable among the cumulus

579   parameters and the application of LTA.

580

581   **6. Discussion and Recommendations**

582   This study corroborated that the simple observation-based LTA scheme implemented in

583   Heath et al. (2016) improved WRF simulated precipitation and other near-surface meteorological

584   variables as evidenced by the simulations over multiple spatial scales and over a longer test

585   period. Testing on a 12-km CONUS domain using lightning flashes from WWLLN instead of

586   NLDN slightly reduced the correlation coefficients and locally increased errors due to the lower

587   detection efficiency of WWLLN. The update of the LTA technique reduced the underestimate of

588   precipitation that was often reported in the application of WRF simulations conducted over the

589   CONUS domain (U.S. EPA, 2019). Changing lightning flash data from NDLN to WWLLN

590   resulted in additional underestimate of precipitation due to fewer lightning flashes in WWLLN

591   than the NLDN dataset. However, when the WWLLN data was used in the hemispheric

592   simulations, the model performance for precipitation over the Equatorial regions was

593   significantly improved from significant overestimation in the base cases to slight

594   underestimation in the LTA cases, and the precipitation over land was generally overestimated

595   during the convective season for almost all the selected regions, especially over North America.

596   The application of LTA in the hemispheric simulations with a 108-km domain exposed a

597   shortcoming of this simple LTA scheme. When the model grid cell is substantially larger than

598   most thunderstorm scales (Murphy and Konrad II, 2005), over-triggering of convection within the

599   entire grid cell leads to overestimated precipitation. With the current LTA implementation and

600   the high lightning detection efficiency network, such as NLDN, the 12-km grid spacing is

601   suitable for LTA because thunderstorms often have a radial distance of 1–10 km. When lightning

602   data from low detection efficiency networks (such as WWLLN) are used over finer resolution

603   domains (≤12 km), the "NoSuppress" option with LTA could balance increasing precipitation

604   while maintaining reasonable levels of uncertainty in the other variables for a more holistic

605   model evaluation. The effect of domain resolution on precipitation simulation with LTA

606   portends further development and improvement of the LTA technique. Two potential

607   developmental directions are to use criteriaalter values of lightning flash density dependent on

608   grid resolution to trigger deep convection and/or to implement the LTA scheme in the MSKF

609   scheme in WRF to adapt to different simulation scales. Preliminary experimentation on the 108-

610   km scale (not shown) suggests that MSKF could improve these comparisons with observations

611 (compared to the KF scheme presented here), including better cloud and precipitation fields

612 (Hogrefe et al., 2021).

613   The experiment of cumulus parameters (trigger and cudt) associated with the KF scheme was

614 performed for both the CONUS and hemispheric WRF simulations. Results revealed several key

615 behaviors in both the BASE case simulations and LTA case simulations. First, the BASE case

616 simulations were sensitive to both trigger and cudt options over the CONUS domain, but only

617 trigger options produced significant variations for the hemispheric simulations. Second, the

618 impact of the cumulus parameters on LTA cases was insignificant for both modeling domains.

619 Separately, the original LTA technique as described in Heath et al. (2016) showed influence

620 from the cumulus parameters on the LTA cases (Figure S8), but after implementing the updated

621 cloud top height (one model level above -20° C) and the additional pre-conditioning shallow

622 convection s of providing a minimum cloud depth as additional deep convection criteria as

623 (seedescribed in Section 2), the fluctuations among the LTA cases were significantly reduced.

624 Third, the most pronounced impact of cumulus parameters was on the amount of precipitation in

625 the BASE cases. The Trig1 option generated up to a 10% overestimate of month-mean daily

626 precipitation over the CONUS with cudt=0 and an additional 10–15% overestimate with cudt=10

627 during July 2016. With Trig2, the simulated precipitation became underestimated by about 10–

628 15%, with the cudt contributing to ~5% difference; Cudt10 had less underestimate than Cudt0.

629 However, over the hemispheric domain, only the trigger option dramatically affected simulated

630 precipitation; during the summer months (June, July, and August), the Trig2 cases

631 underestimated the mean daily precipitation by up to 40% more than the Trig1 cases that

632 matched the observation-based precipitation products within 10%. In summary, without LTA,

633 the recommended default values (trigger=1 and cudt=0) by WRF documentation remain the best

634 option for both the CONUS and hemispheric simulations to achieve the best model performance,

635 especially for North America, and with LTA, all the options performed equally well.

636   As one of the most prominent meteorological models, WRF has been widely used in a variety

637 of applications from regional to global scales and from weather and climate studies to air

638 pollution transport in air quality forecast and regulatory compliances. It is important to improve

639 the convective processes (e.g., convective transport of air pollutants matching the times and

640 locations of lightning NO_x production) to have more accurate precipitation and other

641 meteorological fields with more resources being available including observational datasets,

642 computing capability, and advanced scheme development. Observation-based data assimilation

643 has been historically proven to be one of the most effective methods to improve model's

644 performance in time and space. This research is emerging to consider and use the lightning

645 observations that have become available in various formats and scales in the past decades to

646 improve convection simulations through LTA. Additional networks of lightning observations

647 and more detailed properties associated with the process of lightning discharge are becoming

648 available (such as the ~~scope~~ strokes per flash, ~~and~~ the strength of lightning energy level, and the

649 separation of cloud-to-ground and inter- or intra-cloud strikes being more accurately quantified,

650 especially with the available satellite lightning products from Geostationary Lightning Mapper

651 (GLM) detection systems borne on the GOES-16 and -17 satellites (Goodman et al., 2013)).

652 Accordingly, lightning assimilation techniques will continue to evolve and build upon the

653 research presented here.

654

Code and data availability

The WRF model is available for download through the WRF website (http://www.wrf-model.org/index.php). The LTA code is not publicly available yet but interested users can contact the corresponding author to acquire the source code. The raw lightning flash observation data can be purchased through Vaisala Inc. (https://www.vaisala.com/en/products/systems/lightning-detection), and the WWLLN raw data are also available for purchase at http://wwlln.net. The immediate data except the lightning flash data behind the figures are available from doi: https://doi.org/10.5281/zenodo.6493145. PRISM Precipitation data for the United States are retrieved from https://climatedataguide.ucar.edu/climate-data/prism-high-resolution-spatial-climate-data-united-states-maxmin-temp-dewpoint and the CPC Global Unified Precipitation data provided by the NOAA/OAR/ESRL PSL, Boulder, Colorado, USA, from their Web site at https://psl.noaa.gov/data/gridded/data.cpc.globalprecip.html. The IMERG data were provided by the NASA/Goddard Space Flight Center's Precipitation Measurement Missions (PMM) Science Team and Precipitation Processing System (PPS), which develop and compute the IMERG as a contribution to GPM, and archived at the NASA GES DISC.

Author contributions. DK conceptualized the study, performed the model simulation and data curation, carried out the analysis, and wrote the paper. NH developed the mechanism and software and wrote the paper. RG prepared the scripts for model simulations and data analysis and edited the paper. TS supervised the research, provided resources, and edited the paper. JP edited the paper.

Competing interests. The authors declare that they have no conflict of interest.

Disclaimer: This paper has been subjected to an EPA review and approved for publication. The views expressed here are those of the authors and do not necessarily reflect the views or policies of the U.S. Environmental Protection Agency (EPA).

Acknowledgement:

We thank Jerry Herwehe and Kiran Alapaty at the EPA for reviewing the paper and providing valuable comments and suggestions. We give our sincere thanks to Dr. Lisa Neef and the other anonymous referee for their comments and many suggested changes that have improved the clarity and readability of this paper significantly. PRISM Precipitation data for the United States are retrieved from https://climatedataguide.ucar.edu/climate-data/prism-high-resolution-spatial-climate-data-united-states-maxmin-temp-dewpoint and the CPC Global Unified Precipitation data provided by the NOAA/OAR/ESRL PSL, Boulder, Colorado, USA, from their Web site at https://psl.noaa.gov/data/gridded/data.cpc.globalprecip.html. The IMERG data were provided by the NASA/Goddard Space Flight Center's Precipitation Measurement Missions (PMM) Science Team and Precipitation Processing System (PPS), which develop and compute the IMERG as a contribution to GPM, and archived at the NASA GES DISC.

References

Abarca, S. F., Corbosiero, K. L., and Galarneau Jr., T. J.: An evaluation of the Worldwide Lightning Location Network (WWLLN) using the National Lightning Detection Network (NLDN) as ground truth, J. Geophys. Res., 115, D18206, doi:10.1029/2009JD013411, 2010.

Allen, D. J., Pickering, K. E., Pinder, R. W., Henderson, B. H., Appel, K. W., and Prados, A.: Impact of lightning-NO on eastern United States photochemistry during the summer of 2006 as determined using the CMAQ model, Atmos. Chem. Phys., 12, 1737–1758, 2012.

Appel, K. W., Gilliam, R. C., Davis, N., Zubrow, A., and S. C. Howard, S. C.: Overview of the Atmospheric Model Evaluation Tool (AMET) v1.1 for evaluating meteorological and air quality models, Environ. Modell. Software, 26, 434–443, doi:10.1016/j.envsoft.2010.09.007, 2011.

Appel, K. W., Bash, J. O., Fahey, K. M., Foley, K. M., Gilliam, R. C., Hogrefe, C., Hutzell, W. T., Kang, D., Mathur, R., Murphy, B. N., Napelenok, S. L., Nolte, C. G., Pleim, J. E., Pouliot, G. A., Pye, H. O., Ran, L., Roselle, S. J., Sarwar, G., Schwede, D. B., Sidi, F. L., Spero, T. L., and Wong, D. C.: The Community Multiscale Air Quality (CMAQ) model versions 5.3 and 5.3.1: system updates and evaluation, Geosci. Model Dev., 14, 2867–2897, https://doi.org/10.5194/gmd-14-2867-2021, 2021.

Asong, Z. E., Razavi, S., Wheater, H. S., and Wong, J. S.: Evaluation of Integrated Multisatellite Retrievals for GPM (IMERG)over Southern Canada against Ground Precipitation Observations:A Preliminary Assessment, J. Hydrometeorology, 18, 1033-1050, https://doi.org/10.1175/JHM-D-16-0187.1, 2017.

Bruning, E. C., Weiss, S. A., and Calhoun, K. M.: Continuous variability in thunderstorm primary electrification and an evaluation of inverted-polarity terminology, Atmos. Res., 135–136, 274–284, doi:10.1016/j.atmosres.2012.10.009, 2014.

Burgesser, R. E.: Assessment of the World Wide Lightning Location Network (WWLLN) detection efficiency by comparison to the Lightning Imaging Sensor (LIS), Q. J. R. Meteorol. Soc. 143: 2809–2817, doi:10.1002/qj.3129, 2017.

Fierro, A. O., Mansell, E. R., Ziegler, C. L., and MacGorman, D. R.: Application of a lightning data assimilation technique in the WRFARW model at cloud-resolving scales for the tornado outbreak of 24 May 2011, Mon. Weather Rev., 140, 2609–2627, 2012.

Fierro, A. O., Clark, A., Mansell, E. R., MacGorman, D. R., Dembek, S. R., and Ziegler, C. L.: Impact of storm-scale lightning data assimilation on WRF-ARW precipitation forecasts during the 2013 warm season over the contiguous United States, Mon. Weather Rev., 143, 757–777, 2015.

Finney, D. L., Doherty, R. M., Wild, O., Huntrieser, H., Pumphrey, H. C., and Blyth, A. M.: Using cloud ice flux to parametrise large-scale lightning, Atmospheric Chemistry and Physics, 14 (23), 12,66512,682, doi:10.5194/acp-14-12665-2014, 2014.

Gan, R., Yang, Y., Xie, Q., Lin, E., Wang, Y., and Liu, P.: Assimilation of Radar and Cloud-to-Ground Lightning Data Using WRF-3DVar Combined with the Physical Initialization Method—A Case Study of a Mesoscale Convective System. J. Meteorol. Res. 35, 329–342. https://doi.org/10.1007/s13351-021-0092-4, 2021.

Giannaros, T. M., Kotroni, V., and Lagouvardos, K.: WRF-LTNGDA: A lightning data assimilation technique implemented in the WRF model for improving precipitation forecasts, Environ. Modell. Software, 76, 54–68, 2016.

Gilliam, R. C., Herwehe, J. A., Bullock, Jr, O. R., Pleim, J. E., Ran, L., Campbell, P. C., & Foroutan, H.: Establishing the suitability of the model for prediction across scales for global retrospective air quality modeling. J. Geophys. Res.: Atmospheres, 126, e2020JD033588, https://doi.org/10.1029/2020JD033588, 2021.

Glotfelty, T., Alapaty, K., He, J., Hawbecker, P., Song, X., and Zhang, G.: The Weather Research and Forecasting Model with Aerosol–Cloud Interactions (WRF-ACI): Development, evaluation, and initial application, Mon. Wea. Rev., 147, 1491–1511, doi:10.1175/MWR-D-18-0267.1, 2019.

Goodman, S. J., Blakeslee, R. J., Koshak, W. J., Mach, D., Baiely, J., Buechler, D., Carey, L., Schultz, C., Bateman, M., McCaul Jr., E., and Stano G.: The GOES-R Geostationary Lightning Mapper (GLM), Atmos. Res., 125-126, 34-49, doi: 10.1016/j.atmosres.2013.01.006, 2013.

747   Heath, N. K., Pleim, J. E., Gilliam, R. C., and Kang, D.: A simple lightning assimilation technique for

748   improving retrospective WRF simulations, J. Adv. Model. Earth Syst., 8, 1806–1824,

749   https://doi.org/10.1002/2016MS000735, 2016.

750   Hogrefe, C., Gilliam, R., Mathur, R., Henderson, B., Sarwar, G., Appel, K. W., Pouliot, G., Willison, J.,

751   Miller, R., Vukovich, J., Eyth, A., Talgo, K., Allen, C., and Foley, K.: CMAQv5.3.2 ozone

752   simulations over the Northern Hemisphere: model performance and sensitivity to model

753   configuration. 20th Annual CMAS Conference, November 1–5, 2021, Virtual, 2021.

754   Huffman, G. J., Adler, R. F., and Nelkin, E. J.: Integrated Multi-satellitE Retrievalsfor GPM (IMERG)

755   technical documentation. NASA/GSFC Code612 Tech. Doc., 48 pp. [Available online at

756   http://pmm.nasa.gov/sites/default/files/document_files/IMERG_doc.pdf.], 2015.

757   Kain, J. S.: The Kain-Fritsch convective parameterization: An update, J. Appl. Meteorol., 43(1), 170–181,

758   doi:10.1175/1520-0450(2004)043<0170:TKCPAU>2.0.CO;2, 2004.

759   Kain, J.S. and Fritsch, J. M.: A one-dimensional entraining/detraining plume model and its application in

760   convective parameterization, J. Atmos. Sci., 47, pp. 2784-280,1990.

761   Kain, J.S. and Fritsch, J. M.: Convective parameterization for mesoscale models: the Kain–Fritsch

762   scheme, The Representation of Cumulus Convection in Numerical Models, Meteor. Monogr., No. 46,

763   Amer. Meteor. Soc., pp. 165-170, 1993.

764   Kang, D., Mathur, R., Pouliot, G. A., Gilliam, R. C., and Wong, D. C.: Significant ground-level ozone

765   attributed to lightning-induced nitrogen oxides during summertime over the Mountain West States,

766   npj Climate and Atmospheric Science 3, doi: 10.1038/s41612-020-0108-2, 2020.

767   Kang, D., Pickering, K., Allen, D., Foley, K., Wong, D., Mathur, R., and Roselle, S.: Simulating

768   Lightning NO Production in CMAQv5.2: Evolution of Scientific Updates, Geosci. Model Dev. 12,

769   3071-3083, https://doi.org/10.5194/gmd-12-3071-2019, 2019a.

770   Kang, D., Foley, K., Mathur, R., Roselle, S., Pickering, K., and Allen, D.: Simulating Lightning NO

771   Production in CMAQv5.2: Performance Evaluations, Geosci. Model Dev. 12, 4409–4424,

772   https://doi.org/10.5194/gmd-12-4409-2019, 2019b.

773   Lagouvardos, K., Kotroni, V., Defer, E., and Bousquet, O.: Study of a heavy precipitation event over

774   southern France, in the frame of HYMEX project: Observational analysis and model results using

775   assimilation of lightning, Atmos. Res., 134, 45–55,2013.

776   Liu, Y., Warner, T. T., Bowers, J. F., Carson, L. P., Chen, F., Clough, C. A., Davis, C.A., Egeland, C. H.,

777   Halvorson, S. F., Huck Jr., T. W., Lachapelle, L., Malone, R. E., Rife, D. L., Sheu, R. -S., Swerdlin,

778   S. P., and Weingarten, D. S.: The operational mesogamma-scale analysis and forecast system of the

779   U. S. Army Test and Evaluation Command. Part 1: Overview of the modeling system, the forecast

780   products, J. Appl. Meteorol. Climatol., 47, 1077–1092, 2008.

781   Lopez, P.: A lightning parameterization for the ECMWF Integrated Forecasting System, Monthly

782   Weather Review, 144 (9), 30573075, doi:10.1175/mwr-d-16-0026.1, 2016.

783   Ma, L.-M., and Tan, Z. M.: Improving the Behavior of the Cumulus Parameterization for Tropical

784   Cyclone Prediction: Convection Trigger. Atmospheric Research, 92, 190-211.

785   https://doi.org/10.1016/j.atmosres.2008.09.022, 2009.

786   Mach, D. M., Christian, H. J., Blakeslee, R. J., Boccipio, D. J., Goodman, S. J., and Boeck, W. L.:

787   Performance assessment of the Optical Transient Detector and Lightning Imaging Sensor, J. Geophys.

788   Res.,112, D09210, doi:10.1029/2006JD007787, 2007.

789   Mansell, E. R., Ziegler, C. L., and MacGorman, D. R.: A lightning data assimilation technique for

790   mesoscale forecast models, Mon. Weather Rev., 135, 1732–1748, doi:10.1175/MWR3387.1, 2007.

791   Marchand, M. R., and Fuelberg, H. E.: Assimilation of lightning data using a nudging method involving

792   low-level warming, Mon. Weather Rev., 142, 4850–4871, doi:10.1175/MWR-D-14-00076.1., 2015.

793   Murphy, M. J., Cramer, J. A., and Said, R. K.: Recent history of upgrades to the U.S. National Detection

794   Network, J. Atmos. Ocean. Tech., 38, 573-581, doi:10.1175/JTECH-D-19-0215.1, 2021.

795   Murphy, M. S., and Konrad II, C. E.: Spatial and temporal patterns of thunderstorm events that produce

796   cloud-to-ground lightning in the interior southeastern United States, Monthly Weather Review, 133,

797   1417-1420,2005.

798 Preston, A. D., and Fuelberg, H. E.: Improving lightning cessation guidance using polarimetric radar data,

799   Weather Forecasting, 30, 308–328, doi:10.1175/WAF-D-14-00031.1, 2013.

800 Price, C., and Rind D.: A simple lightning parameterization for calculating global lightning distributions,

801   Journal of Geophysical Research: Atmospheres, 97 (D9), 99199933, doi:10.1029/92jd00719, 1992.

802 Rogers, R. F., Fritsch, J. M., and Lambert, W. C.: A simple technique for using radar data in the dynamic

803   initialization of a mesoscale model, Mon. Weather Rev., 128, 2560–2574, 2000.

804 Romps, D. M., Seeley, J. T., Vollaro, D., and Molinari, J.: Projected increase in lightning strikes in the

805   United States due to global warming, Science, 346 (6211), 851854, doi:10.1126/science.1259100,

806   2014.

807 Rudlosky, S. D., and Shea, D. T.: Evaluation WWLLN performance relative to TRMM/LIS, Geophys.

808   Res. Lett., 40, 2344-2348, doi:10.1002/grl.50428, 2013.

809 Sims, A. P., Alapaty, K., and Raman, S.: Sensitivities of Summertime Mesoscale Circulations in the

810   Coastal Carolinas to Modifications of the Kain-Fritsch Cumulus Parameterization, Mon. Wea. Rev.,

811   145, 4381-4399, doi:10.1175/MWR-D-16-0047.1, 2017.

812 Skamarock, W. C., and Klemp, J. B.: A time-split nonhydrostatic atmospheric model, Journal of

813   Computational Physics, 227, 3465-3485, doi:10.1016/j.jcp.2007.01.037, 2008.

814 Stolzenburg, M., and Marshall, T. C.: Electric field and charge structure in lightning-producing clouds,

815   Lightning: Principles, Instruments and Applications, H.-D. Betz, U. Schumann, P. Laroche (Eds.),

816   641 pp., Springer, doi:10.1007/978-1-4020-9079-0_3, 2009.

817 U.S. EPA: Meteorological Model Performance for Annual 2016 Simulation WRF v3.8, EPA-454/R-19-

818   010, https://www.epa.gov/sites/default/files/2020-10/documents/met_model_performance-

819   2016_wrf.pdf, 2019.

820 Zheng, Y., Alapaty, K., Herwehe, J. A., Del Genio, A. D., and Niyogi, D.: Improving high-

821   resolution weather forecasts using the Weather Research and Forecasting (WRF) Model with

822   an updated Kain–Fritsch scheme, Mon. Wea. Rev., 144, 833–860, doi:10.1175/MWR-D-15-

823   0005.1, 2016.

824

825

Table 1. Model Cases ~~(N/A: Not Applicable)~~**used in this study. The case names are comprised of elements from the other four columns, which describe the simulation domain (blank = CONUS, H = hemispheric), the version of the Kain-Fritsch trigger that was applied (trigger 1 = K1, trigger 2 = K2), the frequency that the convective properties was updated (every time step = C0, every 10 minutes = C10), and the lightning data that were assimilated in the simulation (B = Base/none, N = NLDN, W = WWLLN).**

Case Name	Domain (none or H)	trigger (K1 or K2)	cudt (C0 or C10)	LTA Network (B, N, W)
K1C0B	CONUS	1	0	~~N/A~~Base/none
K1C10B	CONUS	1	10	~~N/A~~Base/none
K2C0B	CONUS	2	0	~~N/A~~Base/none
K2C10B	CONUS	2	10	~~N/A~~Base/none
K1C0N	CONUS	1	0	NLDN
K1C10N	CONUS	1	10	NLDN
K2C0N	CONUS	2	0	NLDN
K2C10N	CONUS	2	10	NLDN
K1C0W	CONUS	1	0	WWLLN
K1C10W	CONUS	1	10	WWLLN
K2C0W	CONUS	2	0	WWLLN
K2C10W	CONUS	2	10	WWLLN
HK1C0B	Hemisphere	1	0	~~N/A~~Base/none
HK1C10B	Hemisphere	1	10	~~N/A~~Base/none
HK2C0B	Hemisphere	2	0	~~N/A~~Base/none
HK2C10B	Hemisphere	2	10	~~N/A~~Base/none
HK1C0W	Hemisphere	1	0	WWLLN
HK1C10W	Hemisphere	1	10	WWLLN
HK2C0W	Hemisphere	2	0	WWLLN
HK2C10W	Hemisphere	2	10	WWLLN

832

833

834

835

836

837

838

839

840

841
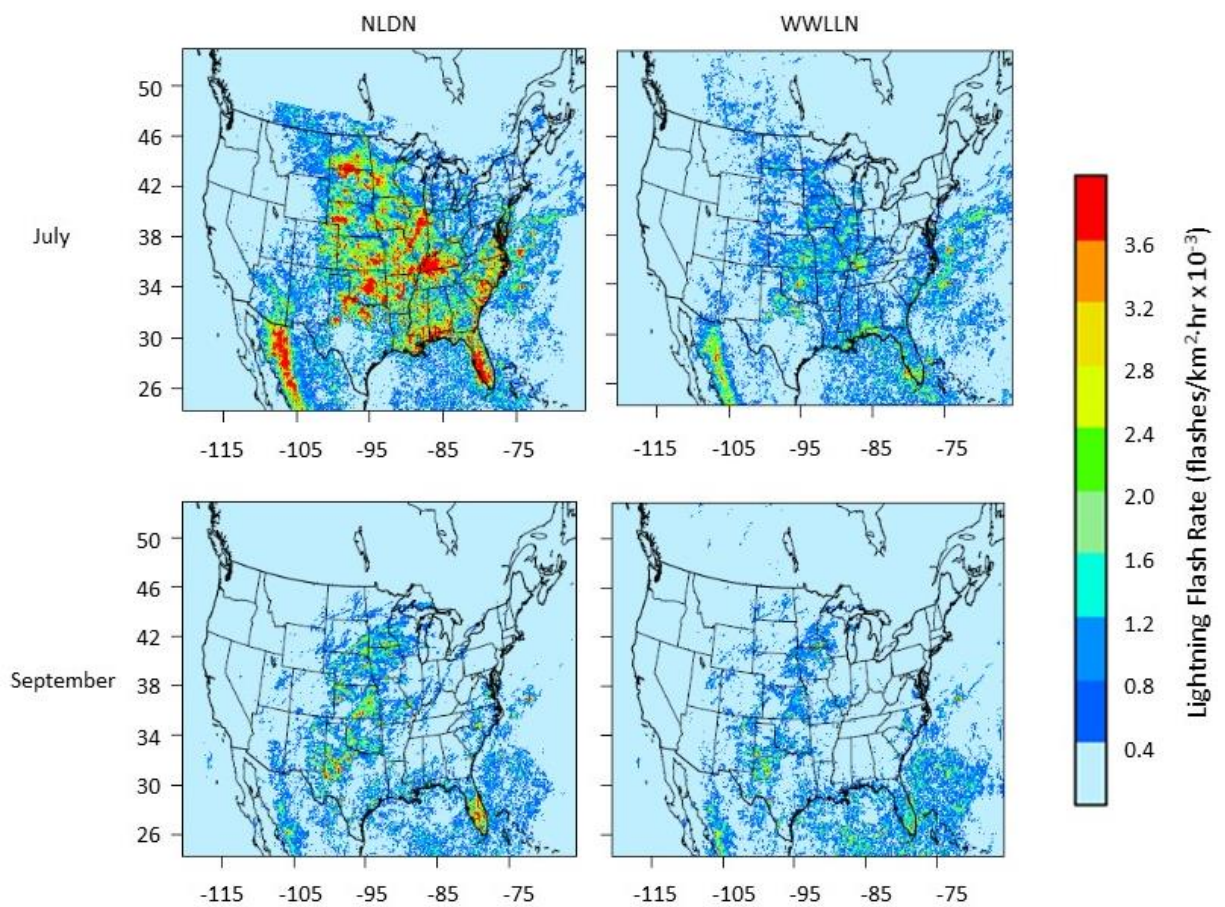
Figure 1. The mean hourly lightning flash rate from NLDN and WWLLN over the 12km

CONUS domain in July and September 2016.

844
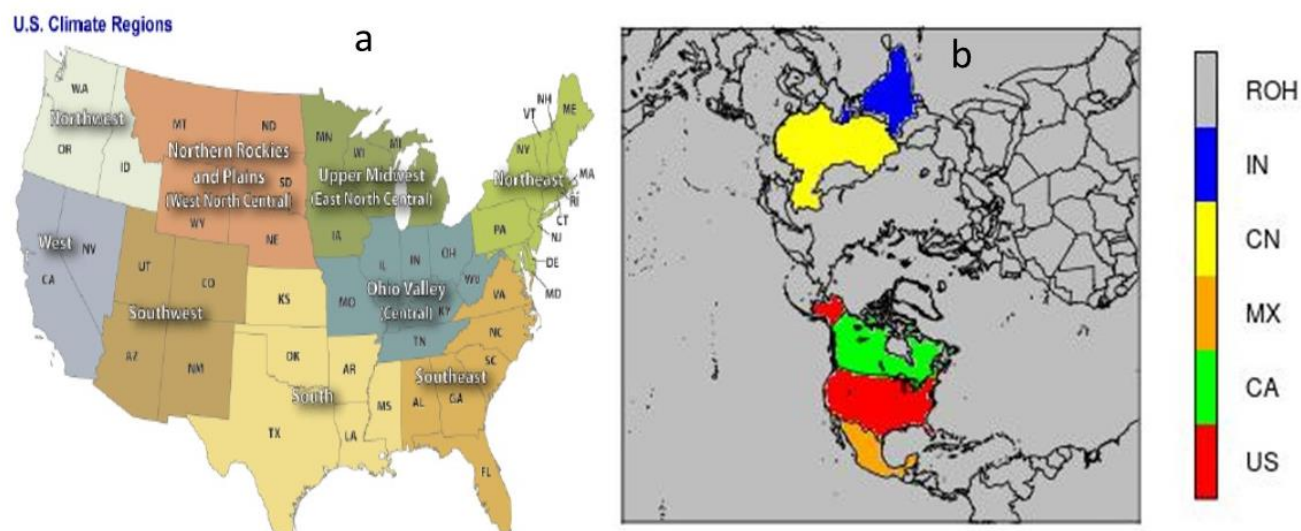
846

847 **Figure 2.** Analysis Regions (Countries), a. the climate regions in the CONUS, and b. the

848 countries over the northern hemisphere – US: United States; CA: Canada; MX: Mexico; CN:

849 China; IN: India; ROH: Other countries/regions except the five specific countries in the

850 hemispheric domain. The U.S. climate regions are: Northeast (NE), Southeast (SE), Ohio Valey

851 Central (OVC), Upper Midwest (UM), South, West North Central (WNC), Southwest (SW),

852 Northwest (NW), and West.

853

854

855
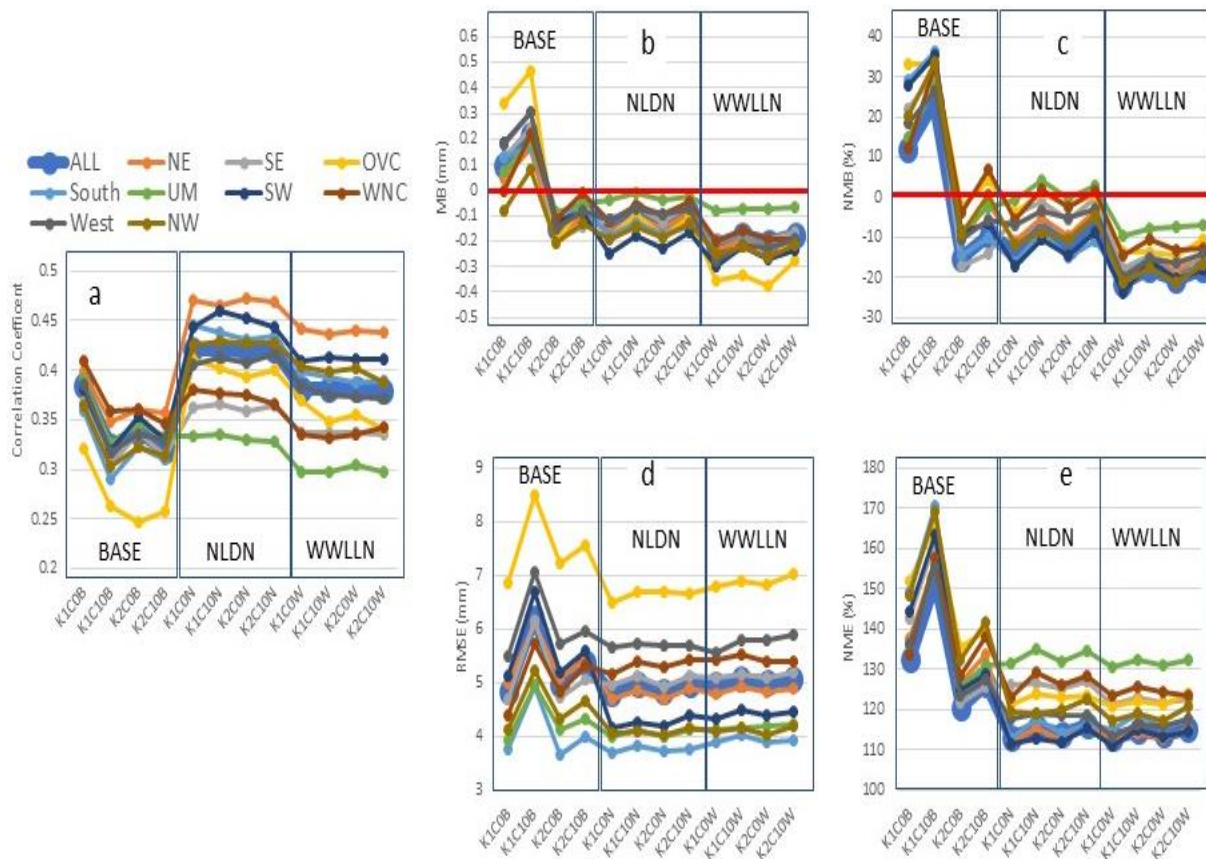
856   **Figure 3.** Monthly mean statistics for precipitation from BASE and LTA simulations

857   comparing to the values from PRISM for the modeling domain and the climatological

858   regions over the CONUS, respectively, during July 2016: a) correlation coefficient, b) MB,

859   c) NMB, d) RMSE, and e) NME. In each plot, there are three sets of simulations (BASE,

860   LTA with NLDN, and LTA with WWLLN) and each having four cases from the

861   combinations of cumulus parameters.

862

863

864
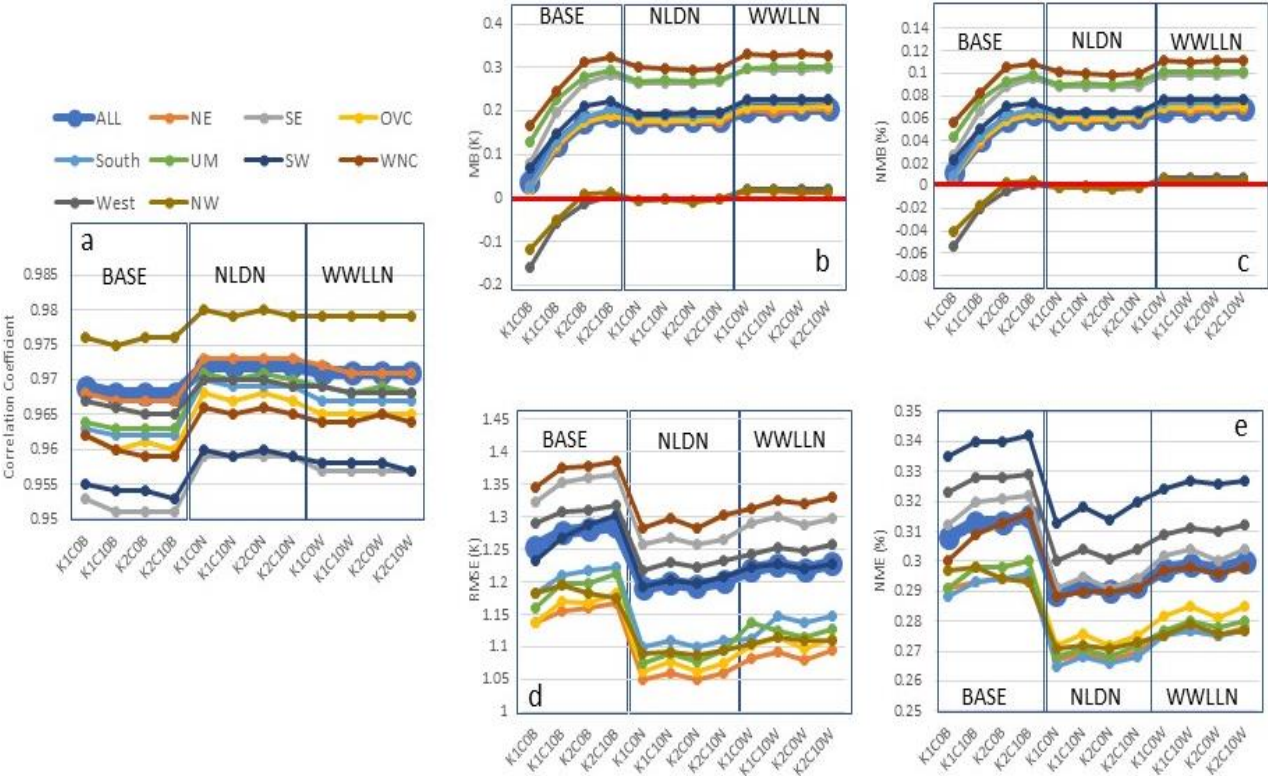
865 **Figure 4.** Same as Figure 3, but for 2-m temperature (T2) in that the simulated T2 values are
866 paired with observations from NCEI's land-based stations in time and space (hourly mean
867 values).

868

42

869

870
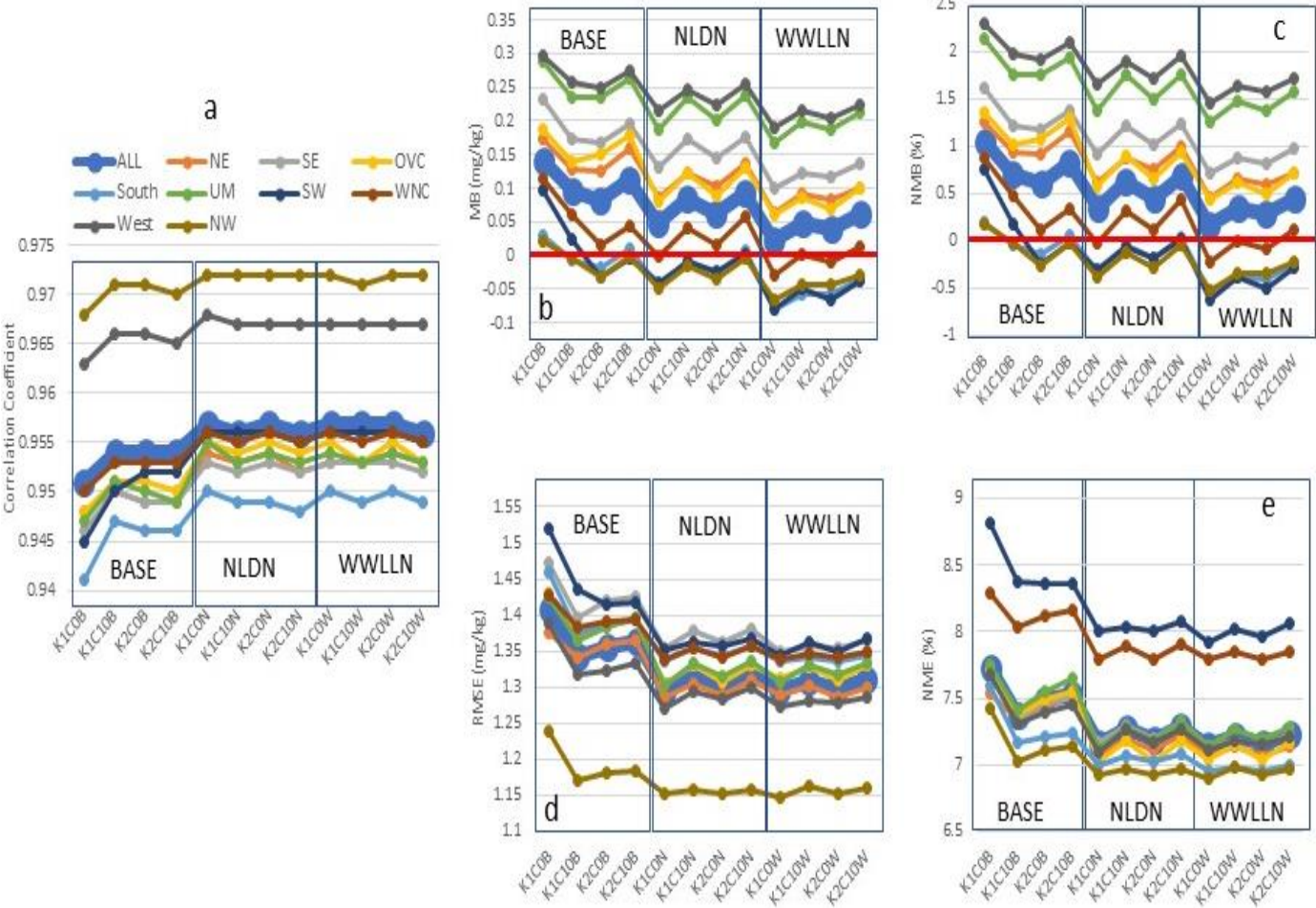
871 **Figure 5.** Same as Figure 4, but for 2-m water vapor mixing ratio.

872

873

874
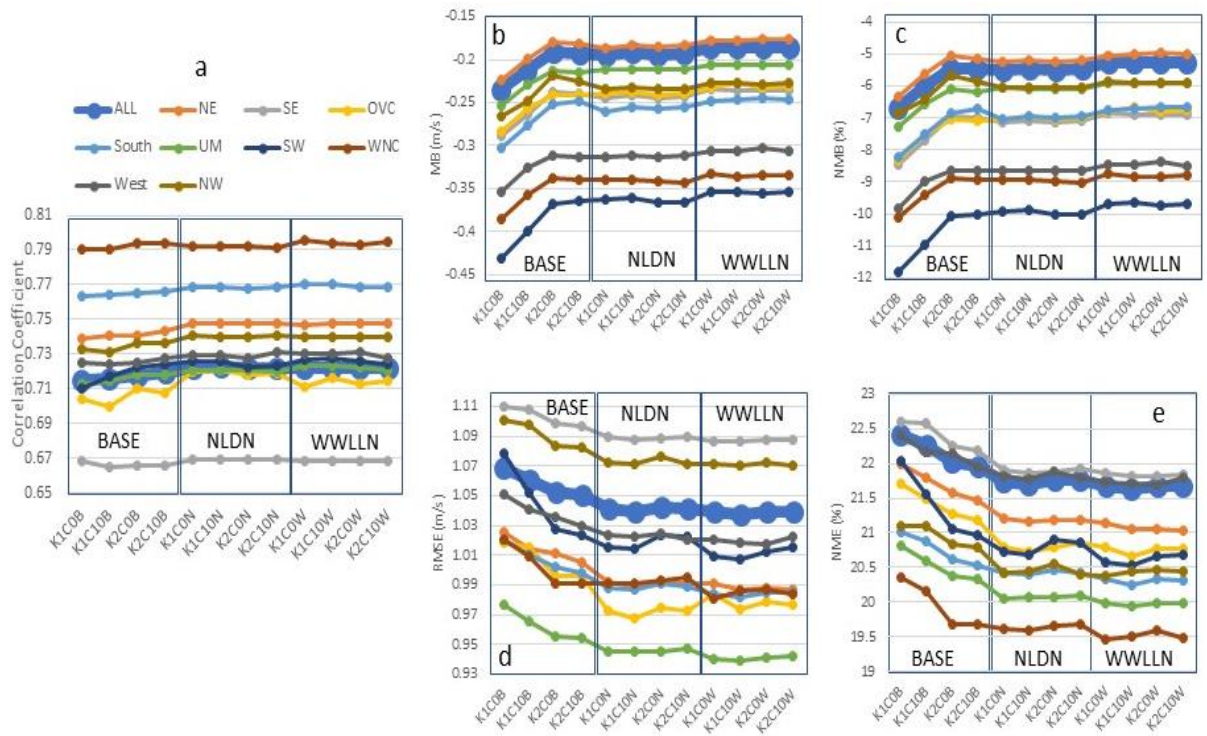
Figure 6. Same as Figure 4, but for 10-m wind speed.

876

877

878

879

880
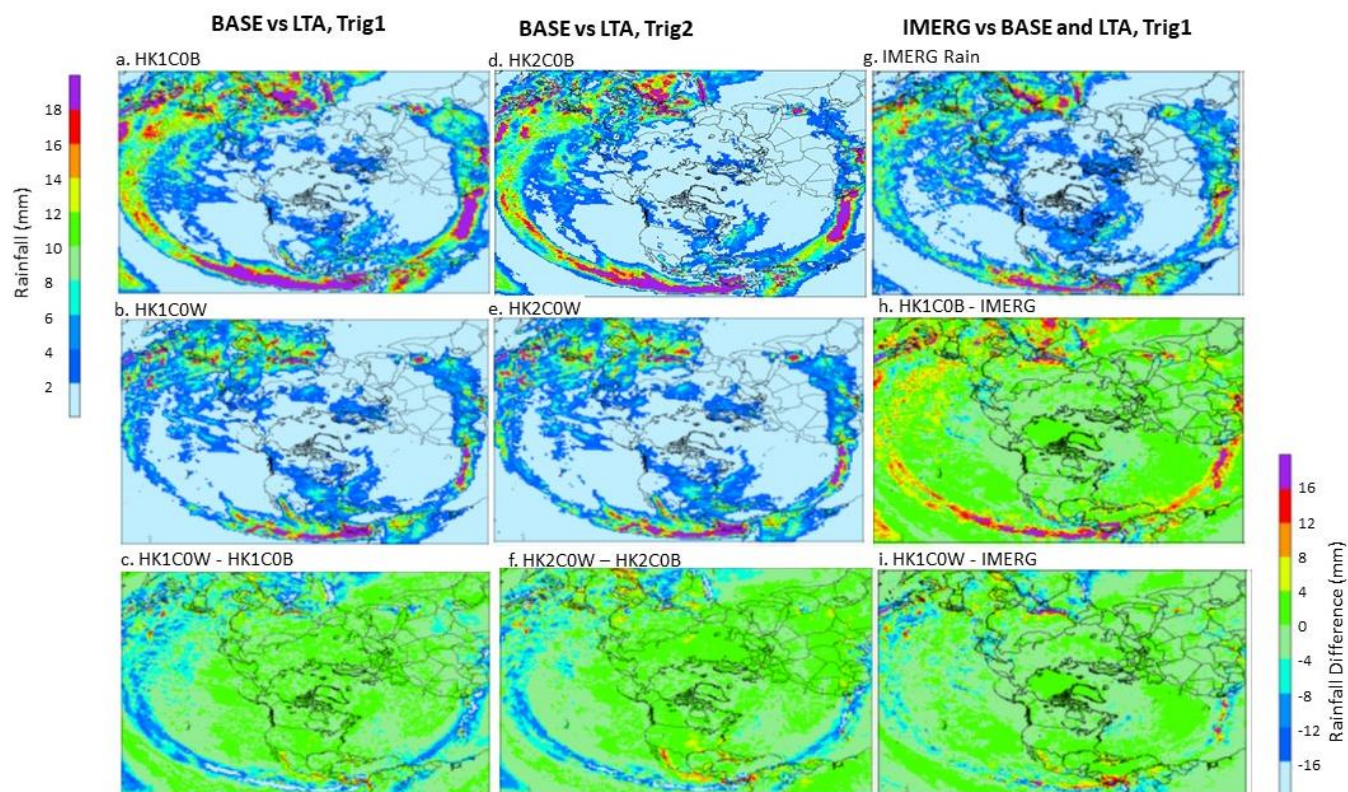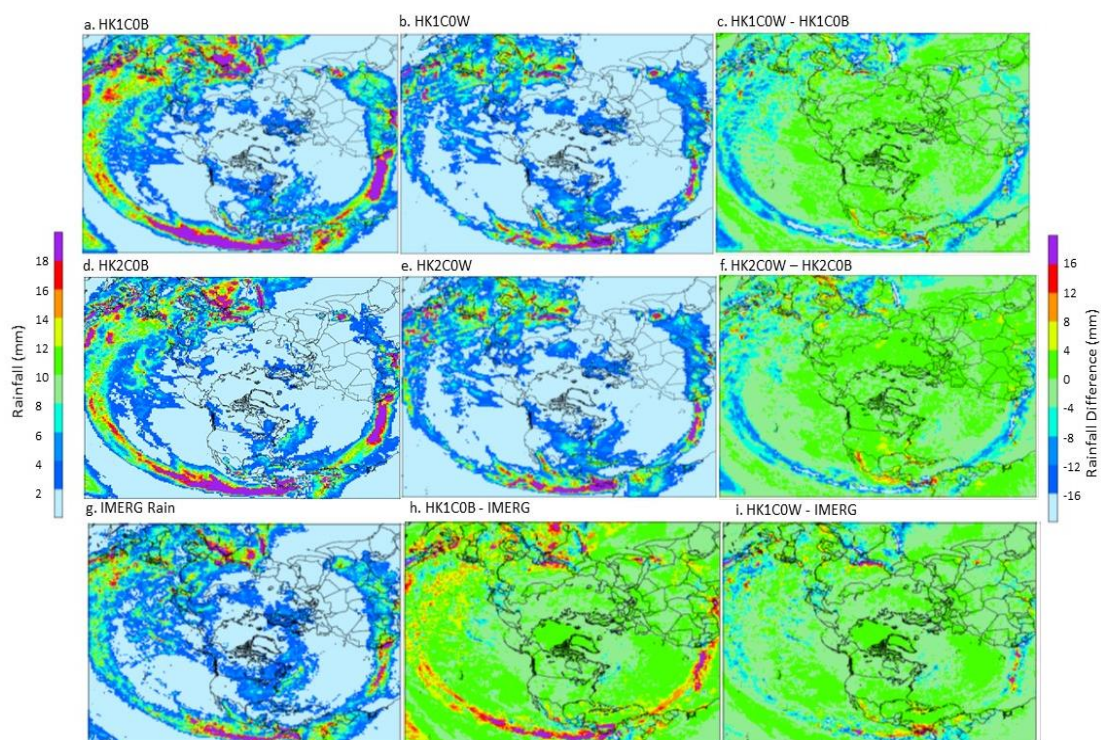
881   **Figure 7**. The mean daily rainfall during July 2016 simulated by base model cases (a. HK1C0B
882   and d. HK2C0B), LTA cases (b. HK1C0W and e. HK2C0W), and the satellite GPM
883   produced rainfall (g), and the differences between the LTA and BASE cases (c.
884   HK1C0W – HK1C0B and f. HK2C0W – HK2C0B) and between the simulated cases and
885   satellite IMERG products (h. HK1C0B – IMERG and i. HK1C0W – IMERG). Note that
886   the left legend applies to the rain maps (a, b, d, e, and g), and the right legend applies to
887   the difference plots (c, f, h, and i).

888

889
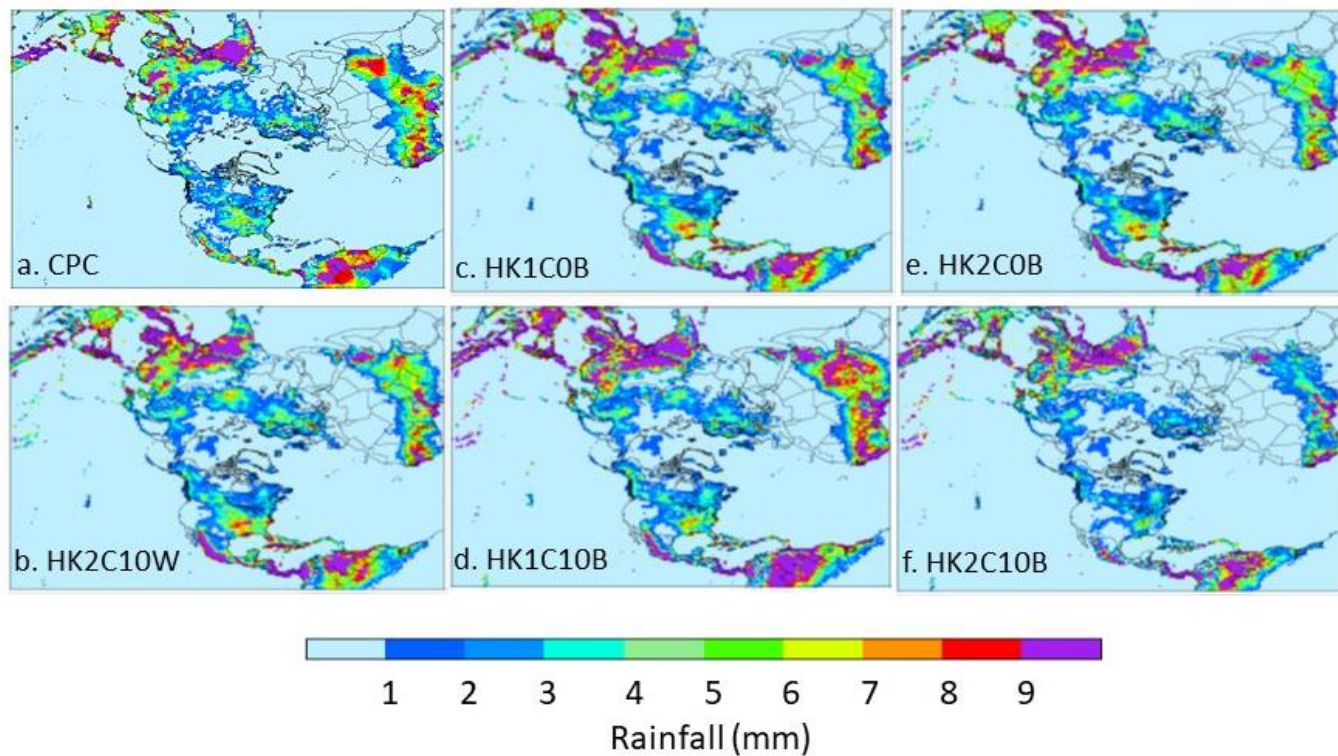
890

891 **Figure 8.** CPC rainfall (a) and simulated (b-f) mean daily precipitation during July 2016 over the
892 hemispheric domain. The LTA configuration is represented by one case (b. HK2C10W) since all
893 the LTA cases with different cumulus parameters produced similar results. All BASE cases are
894 shown here (c-f) because the cumulus parameters do impact the simulated precipitation when not
895 using LTA.

896

897

898
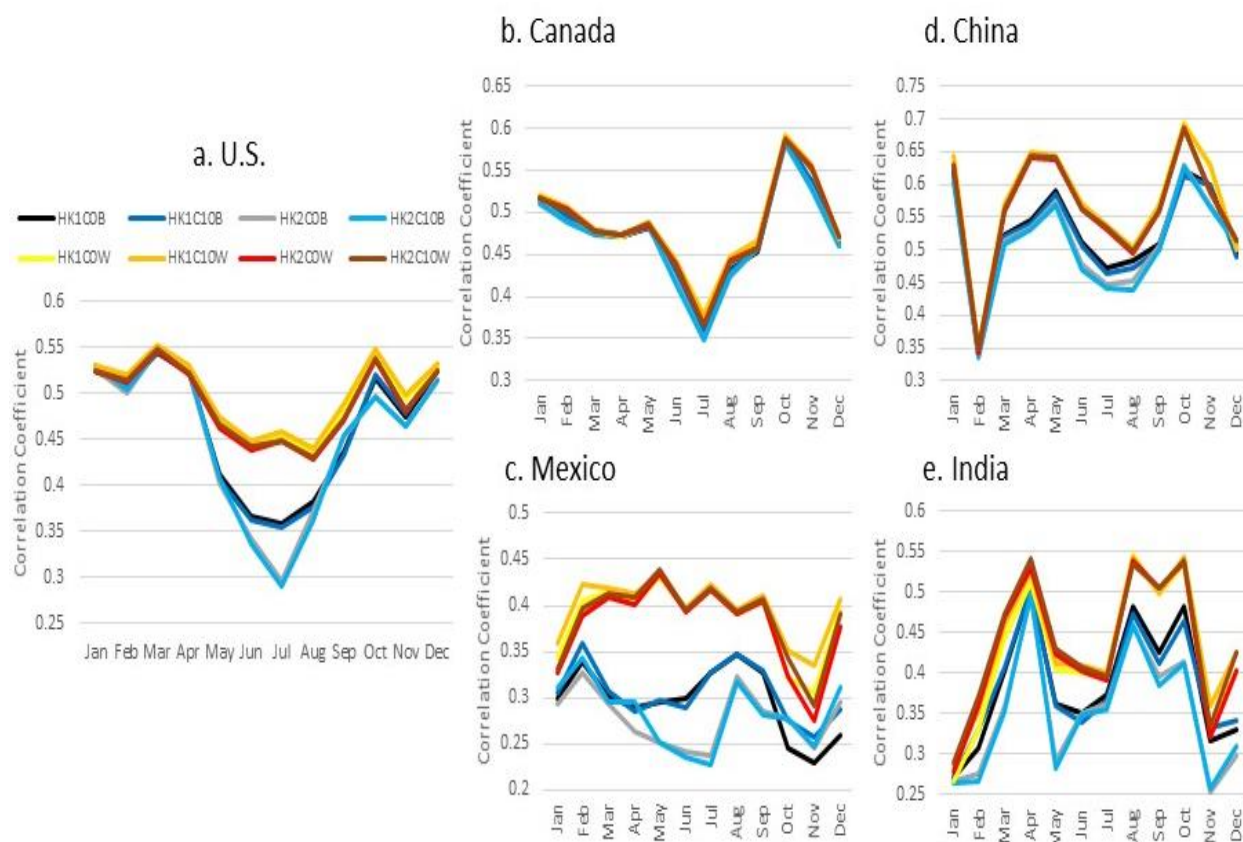
Figure 9. The monthly correlation coefficient between CPC and simulated precipitation in
selected countries: a. United States, b. Canada, c. Mexico, d, China, and e. India. Note
that all the BASE cases are plotted in cool colors and LTA cases in warm colors.

902

903

904

Figure 10. Same as Figure 89, but for RMSE.

906

907

908
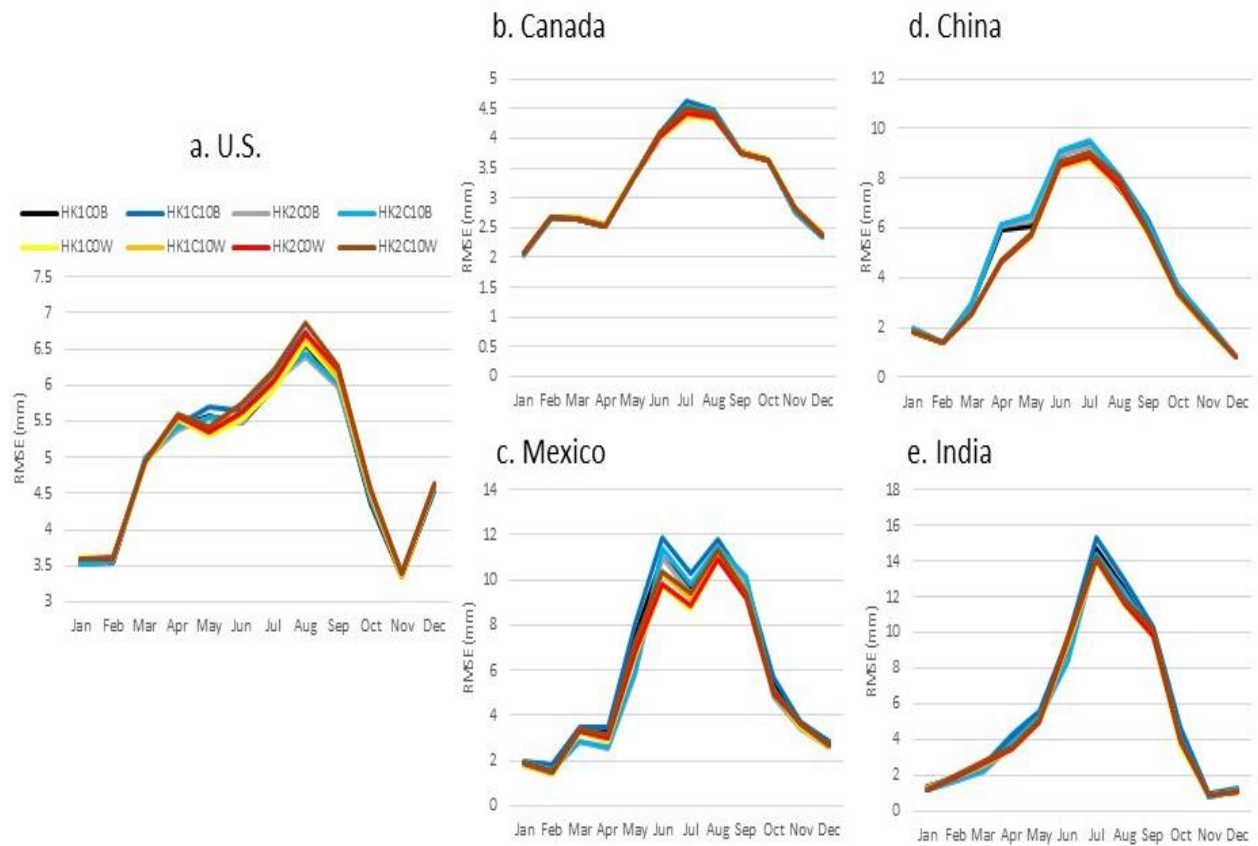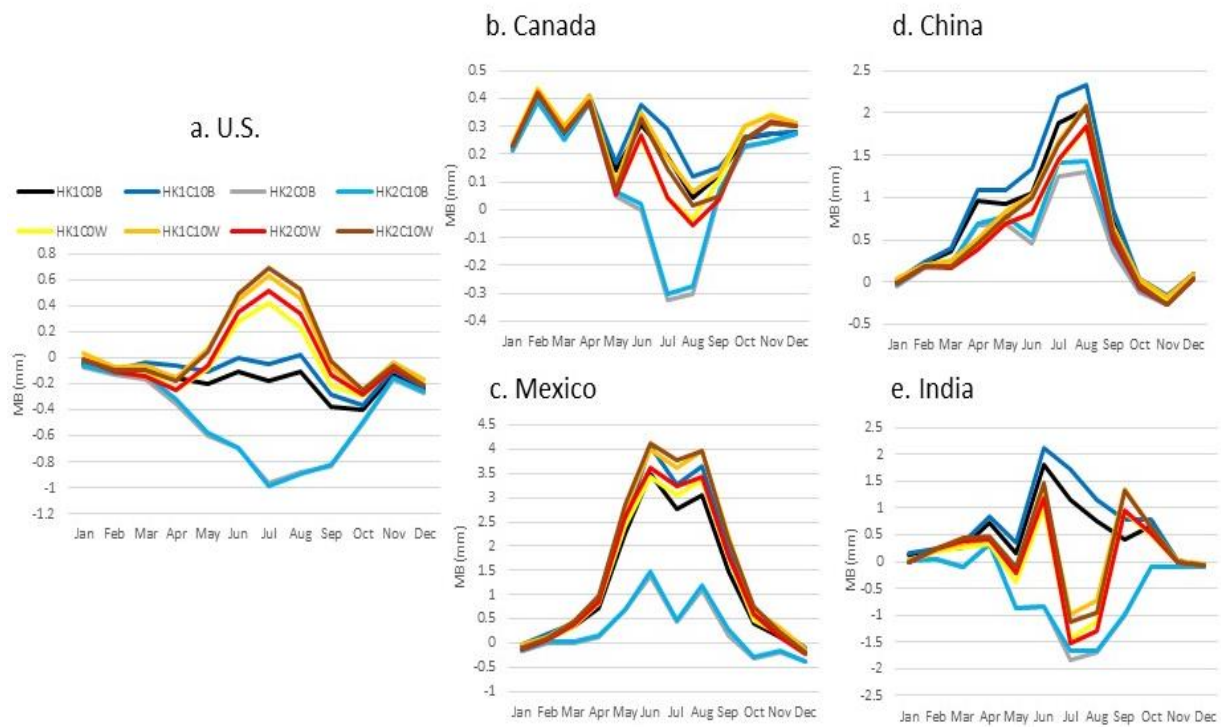
Figure 11. Same as Figure 9, but for MB.

910

911

912
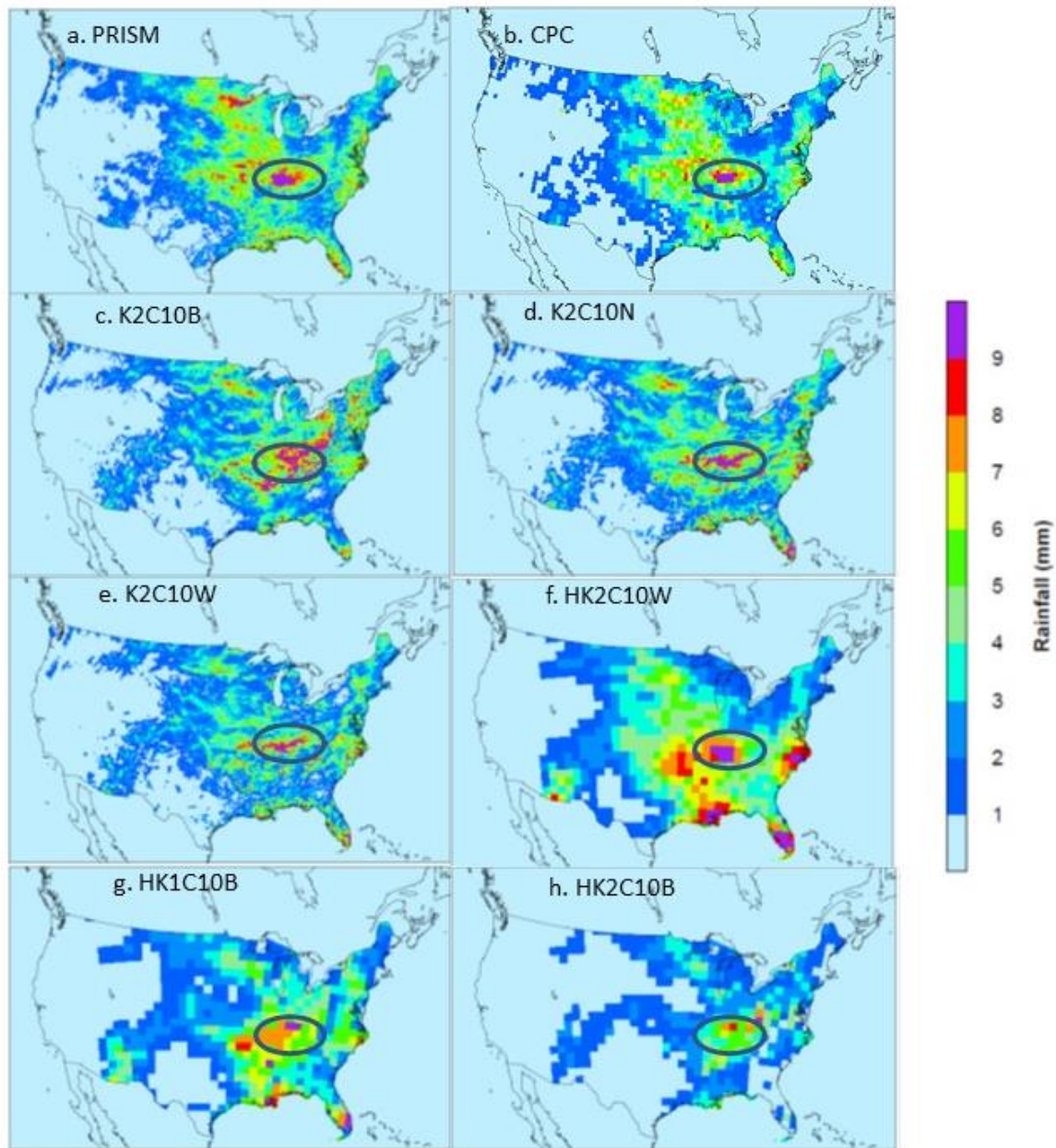
Figure 12. Mean daily precipitation over the CONUS during July 2016 from a) PRISM, b) CPC, c) K2C10B, d) K2C10N, e) K2C10W, and f) HK2C10W, g) HK1C10B, and h) HK2C10B. Note that all the observational based products and the 108 km hemispheric simulations are regridded onto the 12 km CONUS domain.

917

918
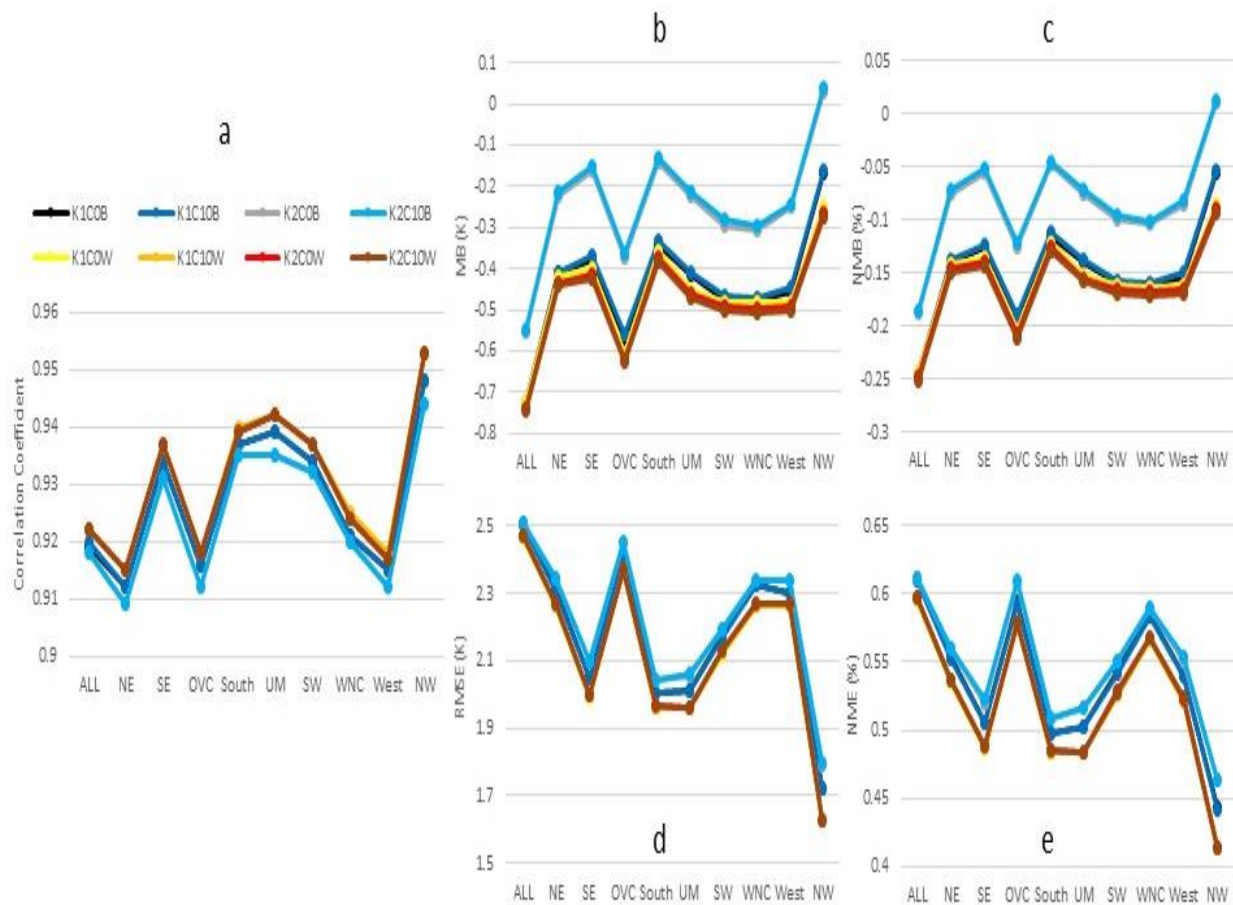
919

920 **Figure 13.** Monthly mean statistics for 2-m temperature from hemispheric BASE and LTA
921 simulations comparing to surface observations during July 2016: a) correlation coefficient, b)
922 MB, c) NMB, d) RMSE, and e) NME.
923

924

925
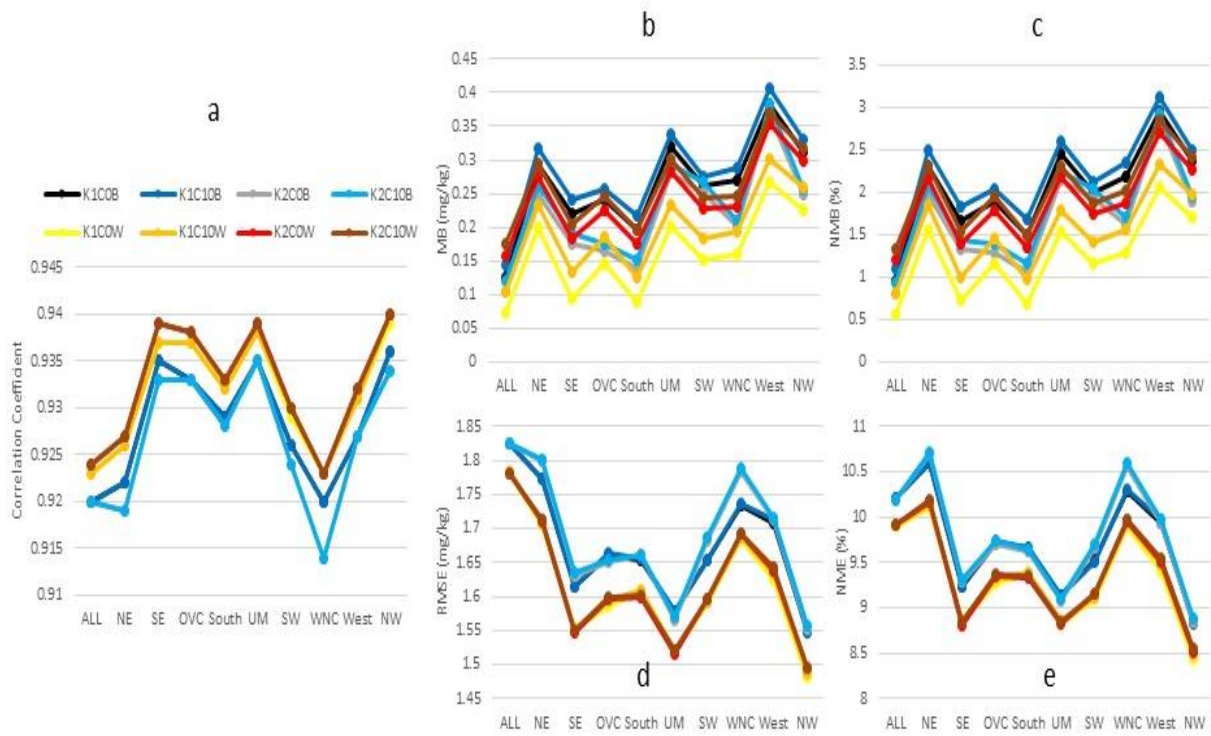
Figure 14. Same as Figure 12, but for 2-m water vapor mixing ratio.

927